VTT Technical Research Centre of Finland

Improving adsorption-based direct air capture performance through operating parameter optimization

Luukkonen, Aaro; Elfving, Jere; Inkeri, Eero

Published in:
Chemical Engineering Journal

DOI:
10.1016/j.cej.2023.144525

Published: 01/09/2023

Document Version
Publisher's final version

Chemical Engineering Journal 471 (2023) 144525

Contents lists available at ScienceDirect

Chemical Engineering Journal

journal homepage: www.elsevier.com/locate/cej

Improving adsorption-based direct air capture performance through operating parameter optimization

Aaro Luukkonen [a,*], Jere Elfving [a], Eero Inkeri [b]

[a] VTT Technical Research Centre of Finland Ltd., Koivurannantie 1, FI-40400 Jyväskylä, Finland
[b] LUT University, School of Energy Systems, Yliopistonkatu 34, FI-53850 Lappeenranta, Finland

ARTICLE INFO

Keywords:
Direct air capture
CO_2 adsorption
Dynamic modelling
Process optimization
Temperature-vacuum swing adsorption
Amine-functionalized adsorbents

ABSTRACT

Direct air capture (DAC) of CO_2 through adsorption is a promising technology for mitigating climate change, but its high cost presents a significant challenge to large-scale implementation. To address this issue, this study presents a dynamic fixed-bed model of the closed-inlet temperature-vacuum swing adsorption (TVSA) process and investigates the impact of various operating and model parameters on DAC performance via dynamic simulation. The results indicate that optimizing the durations of the adsorption and regeneration phases is crucial for improving cyclic DAC performance. Maximizing the working capacity by driving both phases towards near-equilibrium conditions generally leads to the lowest specific energy requirement (SER), while cutting the adsorption phase earlier increases the CO_2 productivity. Additionally, appropriate choices of operating parameters, such as feed gas velocity and vacuum pressure, can significantly improve DAC process performance. Furthermore, placing the DAC unit in a location with favourable temperature and humidity conditions, affordable heat source, and elevated CO_2 concentration can greatly enhance the process and its cost-effectiveness. These individual approaches have the potential to multiply productivity and decrease SER by increasing the working capacity, shortening the cycle duration, and minimizing the absolute energy consumption. However, optimizing the DAC process necessitates careful consideration of trade-offs between productivity, SER, and various constraints. These insights, along with the developed model, can provide a valuable basis for further advancement of DAC technology.

1. Introduction

In recent decades, global annual net anthropogenic greenhouse gas (GHG) emissions have risen dramatically, being the major cause of climate change and global warming [1,2]. CO_2 from fossil fuel combustion and industrial processes make up most of these emissions. The IPCC pathways for limiting warming to 1.5 °C or 2 °C require the implementation of carbon dioxide removal (CDR) from the atmosphere, in addition to substantial direct emission reductions across all sectors, to offset residual GHG emissions and reach net-zero emissions [1].

Direct air capture (DAC) technology, which extract CO_2 directly from the atmosphere using sorbents, is considered as one of the emerging approaches to climate change mitigation [3–5]. Integrated assessment models estimate that DAC is needed to complement other CDR methods at a scale of several Mt/year by 2030 and at a Gt/year-scale by 2050 to limit global warming to sustainable levels [6–8]. Compared to other preferred CDR options, such as bioenergy with carbon capture and storage (BECCS) and afforestation, DAC has a much smaller land and water footprint [9–13]. Moreover, DAC units are location-independent, highly scalable and can capture CO_2 from distributed sources, unlike conventional CO_2 capture technologies that separate CO_2 from large point sources. The captured CO_2 can be stored into geological formations, resulting in negative emissions [14,15]. DAC can also provide a carbon–neutral source of CO_2 for various conversion and utilization pathways, including (1) physical utilization in food, beverage, medicine, oil and gas industries, (2) chemical utilization in the synthesis of fuels, chemicals and polymers, (3) biological utilization in greenhouses and microalgae cultivation, and (4) mineralization utilization, as long as the system is powered by carbon-free energy [16,17].

Two CO_2 capture technologies are commonly used for commercial-scale DAC systems: absorption with aqueous hydroxide solutions and adsorption with solid amine-functionalized adsorbents [18,19]. The absorption-based DAC typically employs solutions of Na, K and Ca hydroxides to capture CO_2 from the air [20–22]. The resulting reaction product is then separated and undergoes a calcium caustic loop to

* Corresponding author.
E-mail address: aaro.luukkonen@vtt.fi (A. Luukkonen).

https://doi.org/10.1016/j.cej.2023.144525
Received 11 May 2023; Received in revised form 28 June 2023; Accepted 29 June 2023
Available online 30 June 2023

Nomenclature

b	adsorption affinity constant (bar^{-1})
b_1	adsorption affinity constant of reaction (1) ($bar^{-1}(mol/kg)^{1-t1}$)
b_2	adsorption affinity constant of reaction (2) ($bar^{-2}(mol/kg)^{1-t2}$)
c	gas-phase concentration ($mol/m^{-3}(-\|-)$)
c_p	specific heat capacity (J kg^{-1} K^{-1})
C	GAB isotherm parameter (–)
C_0	Arrhenius pre-exponential factor to express temperature dependence of C (–)
d	diameter (m)
D_L	axial dispersion coefficient (m^2/s)
E	energy consumption (J)
h	heat transfer coefficient (W m^{-2} K^{-1})
$-\Delta H$	isosteric heat of adsorption (J/mol)
ΔH_C	enthalpy difference between mono- and multilayer adsorption (J/mol)
ΔH_K	enthalpy difference between H_2O condensation and multilayer adsorption (J/mol)
$k_{f,1}$	reaction rate constant for forward reaction (1) ($bar^{-1}s^{-1}(mol/kg)^{1-t1}$)
$k_{f,2}$	reaction rate constant for forward reaction (2) ($bar^{-2}s^{-1}(mol/kg)^{1-t2}$)
$k_{i,LDF}$	linear driving force kinetic constant (s^{-1})
K	GAB isotherm parameter (–)
K_z	axial effective thermal conductivity (W m^{-1} K^{-1})
K_0	Arrhenius pre-exponential factor to express temperature dependence of K (–)
L	length (m)
m	mass (kg)
$\dot{n}$	molar flow rate (m^3/s)
N	number of computational cells (–)
p	pressure (bar)
Δp	pressure drop (bar)
q	adsorption uptake (mol kg^{-1})
q_m	maximum capacity of amines (mol kg^{-1})
$q_{m,mono}$	monolayer adsorption capacity of water in GAB isotherm (mol kg^{-1})
$\overline{q}$	average adsorption uptake (mol kg^{-1})
R	radius (m)
R_{id}	ideal gas constant (J/mol K^{-1})
Re	Reynolds number (–)
RH	relative humidity (%)
t	time (s)
t_1	exponential parameter of reaction (1) (–)
t_2	exponential parameter of reaction (2) (–)
T	temperature (K)
T_0	reference temperature (K)
u	gas velocity (m/s)
V	volume flow rate (m^3/s)
z	axial coordinate (m)

Greek symbols

γ	adiabatic constant (–)
ε	adsorbent bed porosity (–)
η	efficiency (–)
ν	kinematic viscosity (m^2/s)
ρ	density (kg m^{-3})

Subscripts

ads	adsorption
bed	adsorbent bed
CO_2	carbon dioxide
des	desorption
eq	equilibrium
feed	feed gas
g	gas
H_2O	water
i	interstitial
i	index of component
N_2	nitrogen
p	adsorbent particle
react	reaction
s	sorbent/superficial
sen	sensible
sat	saturation
tot	total
vac	vacuum
w	column wall
0	initial condition/reference value
1	reaction (1)/discharge
2	reaction (2)/suction

recover the CO_2. However, the calcination process is highly energy-intensive, leading to the development of alternative solution-based approaches, such as the use of guanidine compounds [23]. In contrast, adsorption-based DAC using amine-functionalized adsorbents has gained more attention due to its generally lower energy requirement for regeneration and better scalability [24–27]. In this approach, CO_2 reacts with amines grafted onto or loaded into porous supports. The adsorbent can be regenerated through various methods, such as increasing the temperature, applying a vacuum, introducing purge gas, or employing a combination of these techniques [28–30]. This work focuses on the widely applied temperature-vacuum swing adsorption (TVSA) process, which produces high-purity CO_2 at mild vacuum and low regeneration temperature of 80–130 °C.

The high cost of DAC has hindered its large-scale implementation, necessitating efforts on process optimization and adsorbent development [13,31–35]. The cost of captured CO_2 varies in the current mid-range estimates, ranging from approximately 100 €/t_{CO2} to 600 €/t_{CO2}, depending on boundary conditions, precision, and underlying assumptions [13,31,33]. However, it is anticipated that the cost will decrease further in the future, potentially falling below 100 €/t_{CO2}.

While many studies have investigated amine-functionalized adsorbents and addressed challenges related to adsorbent design, some parametric and economic assessments have been performed via cyclic simulations of a fixed-bed TVSA process [36–41]. However, these assessments commonly rely on single-component isotherms to describe CO_2 and H_2O adsorption, neglecting the effect of humidity on CO_2 adsorption. In fact, co-adsorption of H_2O can up to double the CO_2 adsorption capacity, underscoring the need for more in-depth consideration of this phenomenon in the optimization process [42,43]. Furthermore, many studies focus on a limited number of operating parameters or on a steam-assisted temperature-vacuum swing adsorption (S-TVSA) process, although the closed-inlet TVSA without steam is also a viable option. Although S-TVSA has been found to increase the working capacity of the DAC process compared to closed-inlet TVSA, it presents challenges such as high energy demand for steam generation and the degradation of some amine-based adsorbents by leaching and structural changes [37,44,45]. For instance, Stampi-Bombelli et al. [37] conducted a comparison between the TVSA cycle with and without steam purge and found that specific energy consumption increased from approximately 10 MJ/kg_{CO2} to 15–40 MJ/kg_{CO2} when different flow rates of

steam purge were applied. Another study by Bos et al. [44] indicated that the implementation of steam purge during desorption could potentially reduce capital expenditure by up to doubling the CO_2 working capacity. However it did not lead to reduced operating expenditures due to the increased specific energy requirement for desorption, which rose from 13 MJ/kg_{CO2} to 13–23 MJ/kg_{CO2} due to the additional heat needed for water evaporation. Therefore, to cut down the cost of DAC via TVSA, it is necessary to undertake a more comprehensive evaluation that considers the impact of a wider range of operating variables and multi-component adsorption.

The primary objective of this research is to analyze the influence of various model parameters and operating parameters on the performance of adsorption-based DAC process in terms of CO_2 productivity and specific energy requirement (SER). The model parameters evaluated include cycle step optimization criteria and heat and mass transfer parameters, while the operating parameters encompass CO_2 concentration, relative humidity, temperature, and superficial velocity of the feed air during adsorption, as well as temperature and vacuum pressure during regeneration. To achieve this goal, a detailed dynamic fixed-bed model of the closed-inlet TVSA process was developed based on the kinetic approach proposed by Elfving and Sainio [46], which accounts for the impact of humidity on CO_2 adsorption. From the previous study [46], the best performing kinetic model was extended with blowdown, heating, and cooling phases for simulating the full TVSA cycle. Furthermore, the model was enhanced with the implementation of an optimization method for determining the optimal durations of cycle steps. The validity of the model is confirmed through a comparison with experimental data. Sensitivity analyses were performed to assess the effect of different parameters on the overall performance of the DAC process. The findings of this study, although specific to the adsorbent and process under investigation, provide valuable insights into optimizing the DAC process for improved CO_2 yield and lower energy consumption. The results can also assist in developing more efficient and cost-effective DAC systems, thereby contributing towards a more sustainable future.

2. Experimental methods

2.1. Materials

A proprietary amine-functionalized polystyrene resin was used for the process analysis of this study, since this material has been characterized in terms of physicochemical structure in Elfving et al. [47] and CO_2 adsorption performance [28,46]. Based on Fourier-transform infrared spectroscopy (FTIR) analysis, the adsorbent is functionalized with primary and secondary amine groups. Elfving [48] and Elfving and Sainio [46] have measured the CO_2 co-adsorption and single-component H_2O isotherms of this adsorbent at various humidity and temperature levels making it possible to accurately model the effect of humidity on the CO_2 adsorption capacity in varying ambient conditions. The applicability of the adsorbent for CO_2 capture from air has been demonstrated using a pilot-scale DAC device consisting of eight beds, with each containing 30 kg of adsorbent [49]. The selection of this adsorbent was based on the abundance of data available on it.

2.2. Experimental setup

The experiments in this study were carried out using an automated fixed-bed adsorption device previously reported in detail by Elfving [48] and Elfving et al. [28]. As a modification to the previous setup, a second column bypass route was installed, as shown in Fig. 1. This alteration

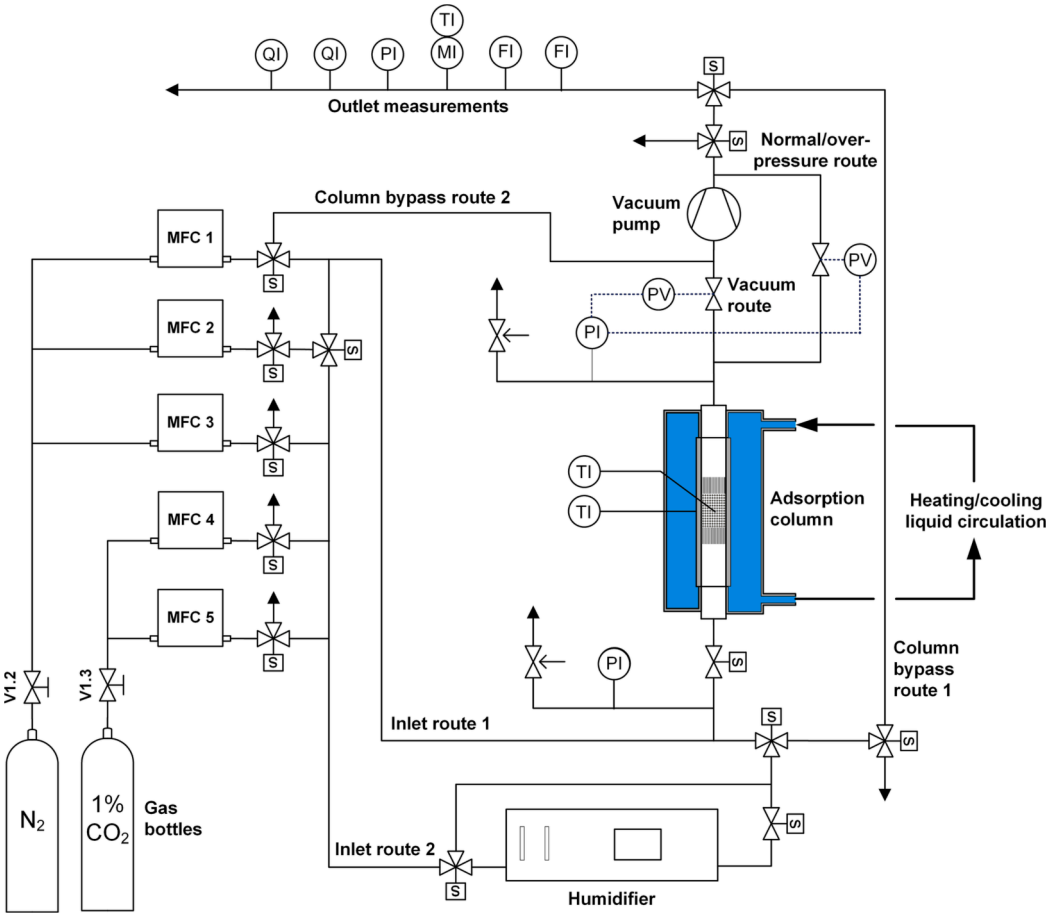

Fig. 1. Experimental setup for fixed-bed CO_2 capture experiments.

enabled flushing of both the vacuum route and the post-column pipeline, improving the measurement accuracy, as explained in Section 2.3. To achieve a flat-bed arrangement with a low pressure drop consistent with the Climeworks' patented design at process scale [50,51], the adsorption column was loaded with 1 g of adsorbent sample, resulting in a bed thickness of 3.3 cm.

2.3. Experiments

The experiments conducted, with the primary purpose of model validation, followed a temperature-vacuum swing (TVSA) cycle with the column inlet closed during regeneration phase. The experimental cycle comprised of four steps: (1) pre-desorption, (2) adsorption, (3) blowdown and (4) desorption by heating.

In the first step, the loaded adsorbent sample was completely regenerated by heating the column to 100 °C while purging with N_2 and applying a vacuum of 50 mbar to remove pre-adsorbed CO_2 and H_2O. At the end of this step, the CO_2 and H_2O concentrations at the outlet were zero. The dry weight of the sample used for capacity calculations was determined by subtracting the mass of pre-adsorbed gas components from the mass measured before loading the sample into the column.

The adsorption step was carried out at ambient conditions by supplying approximately 400 ppm CO_2 balanced with N_2 at a flow rate of 0.5 L/min into the column for 5 h. The H_2O concentration was varied between 0 and 2 vol-% depending on the case.

The adsorption step was followed by a blowdown step, in which the column inlet was closed, and the column pressure was lowered to 12 mbar by applying a vacuum. This step removed N_2 from the column and partly desorbed the adsorbed H_2O from the sample, if present during the adsorption step. A few percent of CO_2 was also lost in the blowdown gas, reducing the CO_2 recovery, but a more throughout blowdown increased the purity of the product. The decision to use such a low vacuum level of 12 mbar was necessitated by the limitations imposed by the oversized vacuum pump used in the experimental setup, which lacked the capability to adjust to a more moderate level. As a result, this vacuum level was only employed during experiments and model validation. In subsequent analyses, a higher vacuum level of 0.1 bar was chosen instead.

Finally, the column was heated to 100 °C, and vacuuming was continued until the CO_2 concentration in the product stream was negligible. However, vacuuming alone was insufficient to transport the desorbed gases to the measurements. Therefore, to ensure the detection of all desorbed CO_2 and H_2O by the outlet measurements, the vacuum route was flushed with an N_2 stream of 0.1 L/min at the end of the blowdown and heating steps. A disadvantage of this method is that the actual desorption kinetics of the regeneration phase could not be measured from the gas concentration profiles, because the desorbed gases were measured only after the desorption had taken place. Table 1 summarizes the experimental conditions for each step.

The experiment-based CO_2 and H_2O adsorption and desorption uptakes were determined by first numerically integrating the outlet concentrations and flow rates to calculate the adsorbed/desorbed volumes of the gas species, and then using ideal gas law to calculate the uptakes. In order to account for the variations in experimental conditions and to align the measurement baselines to zero, appropriate corrections were made to the measured concentrations and flow rates. The data processing and calculation methods are described in more detail in Elfving [28]. The experimental uncertainty in the calculation of uptakes is described in Supplementary Information (SI).

3. Modelling methods

3.1. Isotherm and kinetic models

In this study, a kinetic 7-parameter co-adsorption model developed by Elfving and Sainio [46] was employed to take into account the impact of humidity on CO_2 adsorption. The kinetic 7-parameter model was selected due to its better accuracy in describing the impact of humidity, compared to its simplified variation, so-called 5-parameter model, or the commonly used combination of Toth isotherm and linear driving force (LDF) model. The kinetic model has been derived from the rate equations of CO_2 with primary or secondary amines, assuming a 1:2 molar ratio of captured CO_2 per amine in dry conditions, and 1:1 in humid conditions. Such reaction stoichiometry can be assumed in the formation of ammonium carbamate in dry conditions, and e.g. bicarbonate in humid conditions [18,52–54]. The model was used to gain excellent fits to experimental isotherms with an amine-functionalized resin [46]. The kinetic co-adsorption model consists of separate mass balance equations for the reactions in dry and humid conditions, denoted with subscripts 1 and 2, respectively. By summing these, the total CO_2 adsorption mass balance can be calculated:

$$\frac{dq_{1,CO2}}{dt} = k_{f,1}\left(q_m - 2q_{1,CO2} - q_{2,CO2}\right)^{t_1} p_{CO2} - \frac{k_{f,1}}{b_1} q_{1,CO2} \tag{1}$$

$$\frac{dq_{2,CO2}}{dt} = k_{f,2}\left(q_m - 2q_{1,CO2} - q_{2,CO2}\right)^{t_2} p_{CO2} p_{H2O} - \frac{k_{f,2}}{b_2} q_{2,CO2} \tag{2}$$

$$\frac{dq_{tot,CO2}}{dt} = \frac{dq_{1,CO2}}{dt} + \frac{dq_{2,CO2}}{dt} \tag{3}$$

Two methods for fitting the exponent parameters (t_1 and t_2) of the 7-parameter model were compared in the previous publication [46]. The first method allowed the exponent parameters to freely vary, resulting in the best fit with $t_1 = 10.6$ and $t_2 = 14.4$. Although such high parameter values describe the data better by increasing the order of the model, they also substantially raise the computational effort. Therefore, the second method set upper boundaries of 3 for exponent parameters, leading to optima at their upper limits ($t_1 = t_2 = 3$). Despite this constraint, the 7-parameter model with upper boundaries of 3 provided a considerably better fit than the 5-parameter model, justifying its use in our work.

The temperature-dependent adsorption affinities for the two reaction mechanisms are given by:

$$b_1 = b_{0,1} \exp\left(\frac{-\Delta H_1}{R_{id} T_0}\left(\frac{T_0}{T} - 1\right)\right) \tag{4}$$

Table 1
Experimental conditions of successive cycle steps.

	1. Pre-desorption	2. Adsorption	3. Blowdown	Flush [a]	4. Heating	Flush [a]
Feed	Pure N_2	360 ppm CO_2, 0–2 vol-% H_2O	–	Pure N_2	–	Pure N_2
Feed flow rate	0.1–1 L/min	0.5 L/min	–	0.1 L/min	–	0.1 L/min
Temperature	100 °C	25 °C	25 °C	–	100 °C	–
Pressure	0.05–1.06 bar	1.06 bar	0.012 bar	–	0.012 bar	–
Step time	2.5 h	5 h	0.5 h	0.5 h	2.5 h	1.5 h

[a] Flushing of the vacuum route is conducted at the end of blowdown and heating steps, with the column outlet kept closed to ensure the integrity of the adsorbent bed.

Table 2
Fitted parameters of the kinetic co-adsorption model, GAB isotherm model, as well as CO_2 and H_2O adsorption kinetics [48].

	Parameter	Value
Kinetic co-adsorption model		
	q_m (mol_{amine}/kg)	2.63
	$b_{0,1}$ ($bar^{-1}(mol/kg)^{1-t1}$)	400.39
	$b_{0,2}$ ($bar^{-2}(mol/kg)^{1-t2}$)	$2.38 \cdot 10^4$
	$-\Delta H_1$ (kJ/mol)	84.35
	$-\Delta H_2$ (kJ/mol)	124.02
	t_1 (–)	3
	t_2 (–)	3
CO_2 kinetics		
	$k_{f,1}$ ($bar^{-1}s^{-1}(mol/kg)^{1-t1}$)	0.10–0.34 [a]
	$k_{f,2}$ ($bar^{-2}s^{-1}(mol/kg)^{1-t2}$)	1.60–12.81 [a]
GAB isotherm model		
	$q_{m,mono}$ (mol/kg)	2.58
	C_0 (–)	0.15
	K_0 (–)	0.87
	ΔH_C (kJ/mol)	6.63
	ΔH_K (kJ/mol)	0
H_2O kinetics		
	$k_{H2O,LDF}$ (1/s)	0.16[b]

[a] From correlations (see Figs. S1 and S2 in the SI).
[b] Fitted, not from [48].

$$b_2 = b_{0,2}\exp\left(\frac{-\Delta H_2}{R_{id}T_0}\left(\frac{T_0}{T}-1\right)\right) \quad (5)$$

Kinetics of H_2O adsorption was modelled using the linear driving force (LDF) model [55]:

$$\frac{d\overline{q}_{H2O}}{dt} = k_{H2O,LDF}\left(q_{H2O,eq} - \overline{q}_{H2O}\right) \quad (6)$$

The equilibrium adsorption capacity of H_2O was calculated by the Guggenheim Anderson De Boer (GAB) isotherm model, where the parameters C and K are temperature-dependent [56]:

$$q_{H2O} = \frac{q_{m,mono}CK\left(p_{H2O}/p_{H2O,sat}\right)}{\left(1-K\left(p_{H2O}/p_{H2O,sat}\right)\right)\left(1+K\left(p_{H2O}/p_{H2O,sat}\right)(C-1)\right)} \quad (7)$$

$$C = C_0\exp\left(\frac{\Delta H_C}{R_{id}T}\right) \quad (8)$$

$$K = K_0\exp\left(\frac{\Delta H_K}{R_{id}T}\right) \quad (9)$$

The kinetic and isotherm parameter fitting was not in the scope of this study, so the values previously reported by Elfving [48] for the same adsorbent were used. These values are compiled in Table 2. However, in case of the H_2O kinetic constant ($k_{H2O,LDF}$), a value of 0.16 1/s was gained from re-fitting the current model to experimental breakthrough data of CO_2 adsorption from 400 ppm at 25 °C and 2 vol-% humidity. The same value was used at each humidity condition in this study since no observable difference occurred in the H_2O adsorption breakthrough curve even if this value was increased. Therefore, the adsorption of H_2O was found to be equilibrium-controlled in the studied cases. In this work, the effect of different humidity conditions on DAC are simulated, which is why it was necessary to correlate the reaction rate coefficients of the co-adsorption model with variable relative humidity. The correlations were gained using polynomial regressions on the forward kinetic constants $k_{f,1}$ and $k_{f,2}$ from Elfving [48] at three different humidity levels at 25 °C, corresponding to 7%, 34% and 67% relative humidity (see Table S3 in the SI). These correlations are visualized in Figs. S1 and S2 in Supplementary Information. Using these correlations yields more accurate estimates for kinetic coefficients across different humidity levels compared to constant values that are typically used in simulations. However, it should be noted that the effects of temperature and gas velocity on mass transfer were not taken into account. To ensure a comprehensive analysis, the effects of reaction rate coefficients on process performance are assessed in Fig. 6 in Section 4.2.

3.2. Dynamic fixed-bed model

In a high-performance DAC system, it is essential that the pressure drop is maintained at low levels even at high air flows without sacrificing the capacity of the system. If the adsorbent is applied as a porous bed, the bed geometry must be flat, leading to challenges in the design of the DAC device and the beds to maximize CO_2 capture capacity. An example of smart bed design has been reported in patents filed by Climeworks, which comprises of several parallel-stacked adsorbent-containing layers with thickness of 0.5–5 cm [50,51]. The bed thickness

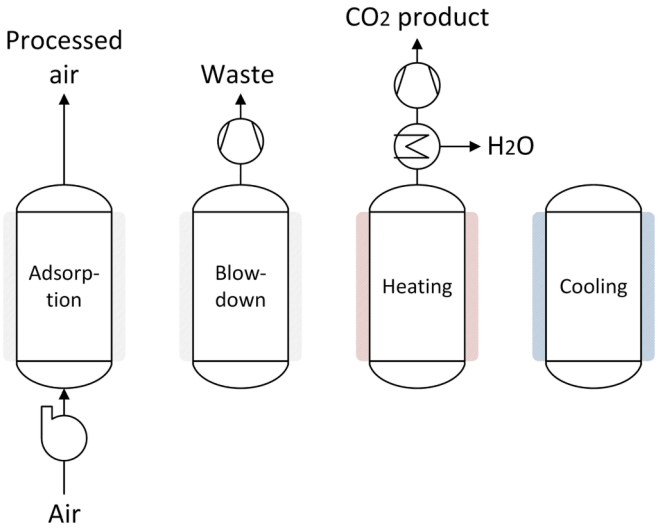

Fig. 2. A schematic of the modelled four-step TVSA cycle with closed inlet during regeneration.

selected in the experiments of this study (3.3 cm) thus corresponds well with the contactor design described in these patents, and results in a reasonably low pressure drop of 260 Pa using the Ergun equation and superficial gas velocity of 0.13 m/s. For comparison, a pressure drop of around 450 Pa was measured during adsorption in the pilot-scale DAC device using the same amino resin [49]. Therefore, the studied system can be assumed to represent a realistic example of process-scale DAC design and was thus used as the base case in the DAC simulation in this work.

A one-dimensional dynamic fixed-bed model was used to simulate the cyclic temperature-vacuum swing adsorption DAC process. The modelled cycle consists of separate steps for adsorption, blowdown, desorption by heating and cooling, as illustrated in Fig. 2.

The adsorbent bed was divided into N number of computational cells in the axial direction. The transient mass and energy balance equations were reduced into a set of ordinary differential equations (ODEs) by discretization of the spatial partial differentials using the finite difference method. This set of ODEs was then integrated using the ODE15s solver in MATLAB. The following assumption were made in the simulation of the studied DAC system:

- The gas flow within the column is represented as an axially dispersed plug flow with no radial concentration, temperature and pressure gradients.
- Only the adsorption of CO_2 and H_2O is considered.
- Constant gas velocity during adsorption. During desorption, gas velocity is calculated using a proportional controller based on the difference between total pressure and vacuum pressure.
- The gas phase is described by the ideal gas law.
- The gas and solid phases are in thermal equilibrium.
- Uniform wall temperature along axial and radial directions.
- Uniform and homogeneous adsorbent packing.

The mass balance for each gas component is given by [57–59]:

$$\frac{\partial c_i}{\partial t} = D_L \frac{\partial^2 c_i}{\partial z^2} - u_i \frac{\partial c_i}{\partial z} - \frac{\rho_{bed}}{\varepsilon} \frac{\partial q_i}{\partial t} \tag{10}$$

The axial dispersion coefficient was calculated using the Chung and Wen empirical correlation [60], where the Reynold's number is $Re = 2R_p u_i \varepsilon / \nu$:

$$D_L = \frac{2R_p u_i \varepsilon}{0.2 + 0.011 Re^{0.48}} \tag{11}$$

A one-dimensional column energy balance is formulated based on the model used by Bollini et al. [57] and Haghpanah et al. [61]. It accounts for convection and diffusion along the axial direction of the bed, heat of adsorption, and heat transfer between the bed and column wall:

$$\left[\rho_g c_{p,g} + \frac{1-\varepsilon}{\varepsilon}\rho_p \left(c_{p,s} + c_{p,CO2} q_{tot,CO2} + c_{p,H2O} q_{H2O}\right)\right] \frac{\partial T}{\partial t} = \frac{1-\varepsilon}{\varepsilon}\rho_p \left[-\Delta H_1 \frac{\partial q_{1,CO2}}{\partial t} - \Delta H_2 \frac{\partial q_{2,CO2}}{\partial t} - \Delta H_{H2O} \frac{\partial q_{H2O}}{\partial t}\right] + K_Z \frac{\partial^2 T}{\partial z^2} - \rho_g c_{p,g} u_i \frac{\partial T}{\partial z} - \frac{2h}{\varepsilon R_{bed}} (T - T_w) \tag{12}$$

The axial effective heat conductivity was estimated as [59]:

$$K_Z = D_L \rho_g c_{p,g} \tag{13}$$

The dynamic model was validated through a comparison of simulation results with experimental data, using the same experimental conditions as model input parameters. Following validation, the model was employed to conduct sensitivity analyses, evaluating the impact of different parameters on the performance of the DAC process. Sensitivity analyses were conducted by varying one parameter at a time within a relevant range, while keeping all other parameters at their predetermined base case values. The base case values used in these analyses were primarily derived from experimental conditions, except for the vacuum pressure. To represent a more practical DAC system, the vacuum pressure was increased from the too low experimental level of 0.012 bar to 0.1 bar in the subsequent sensitivity analyses, based on the considerations presented in Section 2.3. These base case model parameter values are listed in Table 3.

Table 3
Model parameters used in the simulations.

	Parameter	Base case value
Column properties		
	L_{bed} (m)	0.033
	R_{bed} (m)	0.0045
	ρ_{bed} (kg/m^3)	450
	ε (–)	0.375
	N (–)	100
Adsorbent properties		
	m_s (kg)	$0.95 \cdot 10^{-3}$
	R_p (m)	$3 \cdot 10^{-4}$ [47]
	ρ_p (kg/m^3)	720
	$c_{p,s}$ (J/(kg·K))	1580 [62]
Operating conditions		
	T_{feed} (°C)	25
	P_{feed} (bar)	1.01
	V_{feed} (L/min)	0.5
	$u_{s,feed}$ (m/s)	0.131
	$y_{CO2,feed}$ (-)	0.0004
	RH_{feed} (%)	70
	T_{des} (°C)	100
	P_{vac} (bar)	0.1
Heat transfer		
	h (W/(m^{2}K))	27.3
Gas properties		
	ν (m^2/s)	$1.5 \cdot 10^{-5}$
	$c_{p,CO2}$ (J/(kg·K))	844
	$c_{p,H2O}$ (J/(kg·K))	4183
	$c_{p,N2}$ (J/(kg·K))	1040
	$-\Delta H_{H2O,0}$ (kJ/mol)	50.73 [48]
	γ (-)	1.4
Efficiencies		
	η_{fan} (-)	0.6 [39]
	η_{vac} (-)	0.3–0.72 [63]

The performance of the DAC system was primarily evaluated with two key performance indicators (KPIs): CO_2 productivity and specific energy requirement. Productivity depicts the efficiency of the cycle, i.e. how quickly and what proportion of the adsorbent can be used for CO_2 recovery:

$$Productivity = \frac{m_{CO2,product}}{m_s t_{cycle}} \tag{14}$$

Specific energy requirement refers to the amount of energy that is used to produce a kilogram of CO_2. The total SER consists of electrical (SER_{el}) and thermal specific energy consumptions (SER_{th}):

$$SER_{el} = \frac{E_{fan} + E_{vac}}{m_{CO2,product}} \tag{15}$$

$$SER_{th} = \frac{E_{sen,s} + E_{sen,CO2} + E_{sen,H2O} + E_{react,CO2} + E_{react,H2O}}{m_{CO2,product}} \tag{16}$$

$$SER = SER_{el} + SER_{th} \tag{17}$$

Electrical energy is consumed by the air fans during adsorption and the vacuum pump during regeneration, the energy consumption of which were calculated according to the following equations:

$$E_{\text{fan}} = \int_0^{t_{\text{ads}}} \frac{1}{\eta_{\text{fan}}} \Delta p \dot{V}_{\text{feed}} dt \tag{18}$$

$$E_{\text{vac}} = \frac{1}{\eta_{\text{vac}}} \frac{\gamma}{\gamma - 1} \int_0^{t_{\text{des}}} \dot{n} R_{\text{id}} T \left[\left(\frac{p_2}{p_1} \right)^{\frac{\gamma-1}{\gamma}} - 1 \right] dt \tag{19}$$

The efficiency values reported in [39,63] were used to define the performance of these devices. The vacuuming efficiency was varied linearly between 30 and 72% as a function of the targeted vacuum pressure. At very low pressures below 0.02 bar, the estimated efficiency was 30%, while at more practical pressures above 0.1 bar, the efficiency was estimated to be 72%. The pressure drop was estimated using the Ergun equation.

The thermal energy of regeneration consists of the sensible heat of the adsorbent material and desorbing components, as well as the heat absorbed during the desorption reaction of these components:

$$E_{\text{sen,s}} = m_{\text{s}} c_{\text{p,s}} \Delta T \tag{20}$$

$$E_{\text{sen},i} = m_{i,\text{desorbed}} c_{\text{p},i} \Delta T \tag{21}$$

$$E_{\text{react},i} = \int_0^{t_{\text{des}}} -\Delta H_i \dot{n}_i dt \tag{22}$$

In the sensitivity analyses, the cycles were repeated three times, resulting in a change in working capacity of less than 0.005% between the second and third cycles. This approach strikes a balance between reaching an exact cyclic steady state and minimizing computational time. The performance indicators were calculated based on the results of the last cycle.

To establish initial conditions for the first cycle, the adsorbent bed was fully regenerated and set to inert conditions, while the column wall temperature was set to match the feed gas temperature. The initial conditions for the subsequent steps and cycles were based on the final conditions of the previous step. To specify the gas-phase concentrations and temperature at the inlet boundary, Danckwert's boundary conditions were applied. At the outlet, zero concentration and temperature gradients were enforced. Detailed summary of the boundary and simulation conditions for each step can be found in Table S4 in the Supplementary Information.

4. Results & discussion

4.1. Model validation

The dynamic fixed-bed model was validated using experimental data from two experiments with distinct H_2O feed concentrations. In the first case, the feed air was entirely dry, whereas in the second case, the H_2O concentration in the feed was 2 vol-%, which equates to a relative humidity of 67%. The CO_2/H_2O breakthrough and uptake profiles of the adsorption phase, as shown in Fig. 3, indicate that the model accurately predicts the profiles for the dry feed air. It should be noted that the co-adsorption model was fitted with only humid data, imparting that the model extrapolates well at least in lower humidity region. However, with 2 vol-% H_2O the simulated breakthrough takes place too early for both CO_2 and H_2O (Fig. 3a and 3b). The main reason for this is that the model underpredicts the CO_2 and H_2O uptakes, as shown in Fig. 3c and 3d.

The humid case clearly differs from the results presented by Elfving

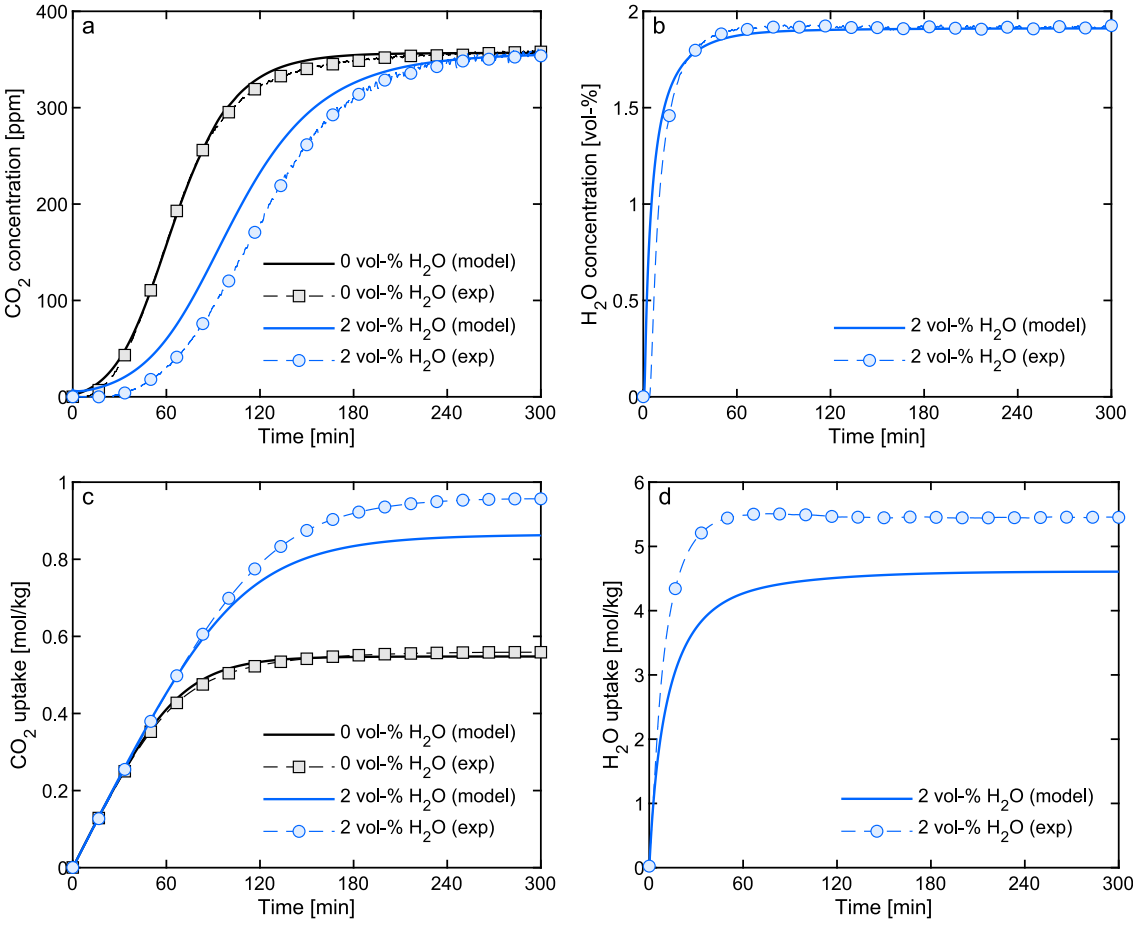

Fig. 3. Experimental and simulated (a) CO_2 breakthrough profiles, (b) H_2O breakthrough profiles, (c) CO_2 uptake profiles and (d) H_2O uptake profiles in the adsorption phase.

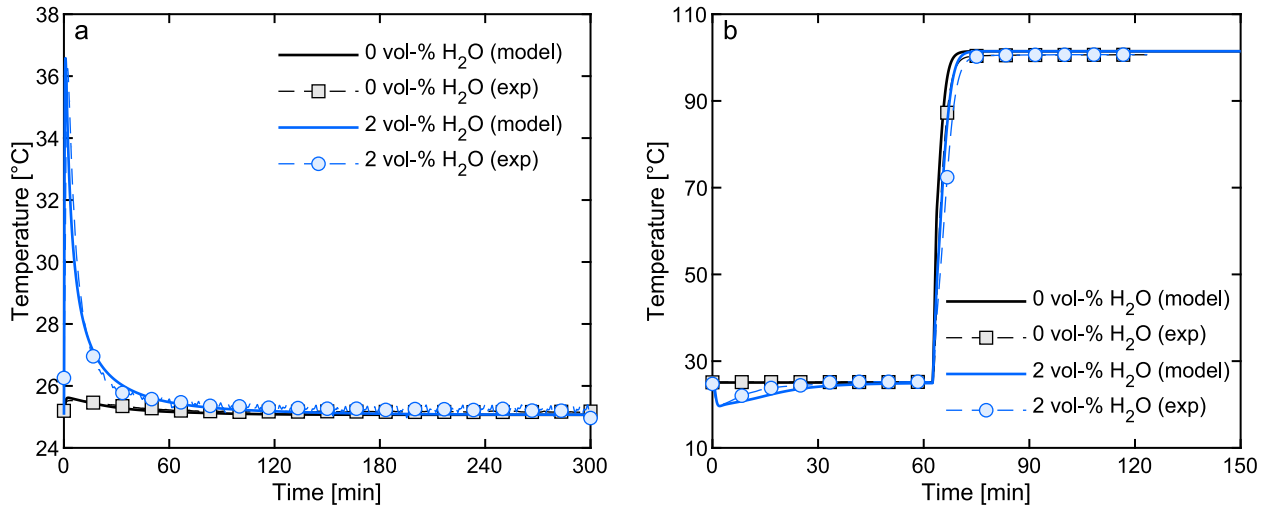

Fig. 4. Experimental and simulated bed temperature profiles for (a) adsorption phase and (b) regeneration phase.

and Sainio [46]. Their study demonstrated that employing a 7-parameter co-adsorption model yielded excellent fits to CO_2 isotherms and breakthrough profiles, particularly at 1–2 vol-% humidity and 25 °C. However, the experiments conducted in this work differ in terms of bed length, which is twice as long as that used in the aforementioned study. Under similar feed conditions, it would typically be expected that the CO_2 and H_2O uptakes would be slightly smaller rather than larger with an extended bed, unless the bed has reached full saturation. To the best of our knowledge, the discrepancy observed can most likely be attributed to the higher uncertainty associated with experiments conducted under humid conditions, particularly concerning H_2O uptake, as depicted in Tables S1 and S2 in the Supplementary Information. Furthermore, the disparities in uptake could also stem from uncertainties originating from the humidity calibrator and possible variations in the adsorbent samples.

In the regeneration phase, the experimental breakthrough and uptake profiles may not be reliable indicators for direct model validation, unlike in the adsorption phase. This is because the measurement of most of the desorbed gas components occurred when the post-column pipeline was flushed with N_2 stream, which does not accurately represent the real desorption kinetics. Instead, the temperature of the bed can be used to describe the desorption behaviour and validate the model. This is because desorption of CO_2 and H_2O are endothermic processes that have significant impact on bed temperature and the desorption rate is ultimately limited by the heat transfer within the bed.

The temperature profiles of the bed, both experimental and simulated, are depicted in Fig. 4. At both humidity levels, the simulated profiles closely resemble the experimental ones. A temperature peak is observed at the beginning of the adsorption phase, because of the exothermic adsorption reactions of CO_2 and H_2O (Fig. 4a). Notably, the effect of H_2O on temperature is more pronounced due to its higher concentration in the feed. Following the peak, the bed temperature returns to the feed temperature. In the regeneration phase, a temperature drop takes place during the blowdown step due to the partial endothermic H_2O desorption. Similarly, the temperature rise during the heating step is constrained by the endothermic desorption reactions and heat transfer limitations, with stronger heat effects observed for 2 vol-% H_2O case (Fig. 4b).

4.2. *Effect of model parameters*

This section evaluates the impact of model parameters, including step optimization criteria and heat and mass transfer parameters, on the key performance indicators. To minimize the cost of CO_2 capture, a mechanism was introduced to optimize the duration of each cycle step. Each step is carried out until a specific criterion is met, which varies depending on the step being executed. This ensures that the steps will not continue longer than necessary. The adsorption step is terminated when the CO_2 loading of the adsorbent reaches a predetermined percentage of the equilibrium adsorption capacity. The blowdown step

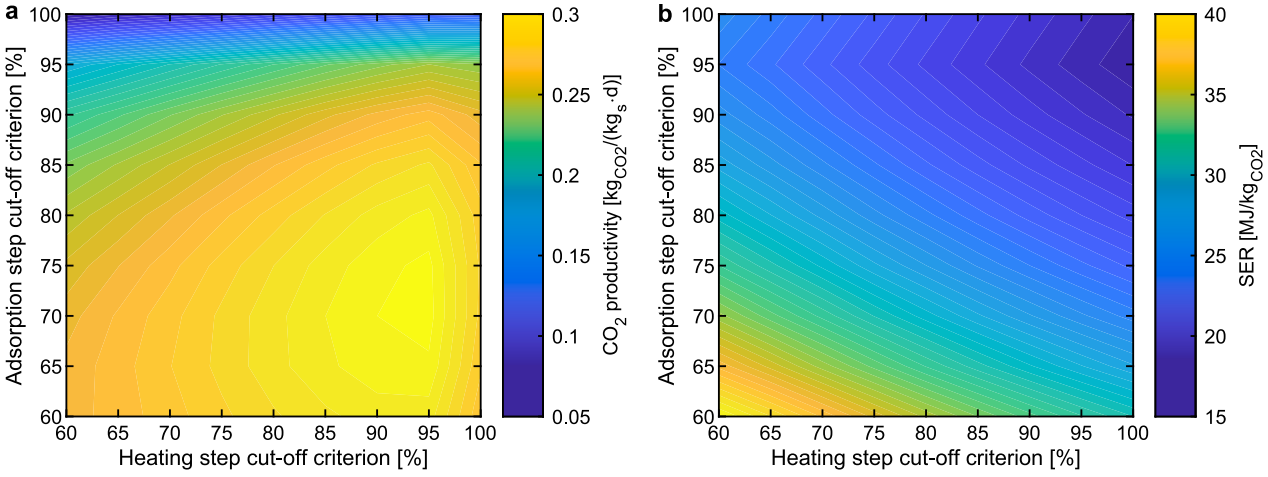

Fig. 5. Effect of adsorption and heating step cut-off criteria on (a) CO_2 productivity and (b) specific energy requirement.

Table 4
Selected cut-off criteria for sensitivity analyses.

Step	Value	Definition
Adsorption	60%, 75%, 90%	The proportion of CO_2 loading of the equilibrium adsorption capacity.
Blowdown	99.9%	The proportion of reached average pressure of the target vacuum pressure.
Heating	95%	The proportion of achieved working capacity of the maximum achievable working capacity within the cycle.
Cooling	90%	The proportion of bed temperature of the adsorption temperature.

following adsorption is halted when the average pressure reaches a target vacuum pressure threshold. The heating step is stopped once the desired share of the maximum working capacity, attainable under the pressure and temperature conditions of the cycle, is achieved. Lastly, the cooling step is ended when 90% of the cooling demand, the difference between adsorption and desorption temperature, is covered.

The cut-off criteria for the blowdown and cooling steps were adjusted based on preliminary simulations as well as design considerations discussed in the literature. Given their much shorter durations and lesser impact on performance, a precise optimization of these steps was considered unnecessary. However, sufficient cooling, close to the feed temperature, was ensured to prevent oxidative degradation of the adsorbent upon exposure to air [64]. Furthermore, the blowdown criterion was set to a sufficiently high level of 99.9% to remove majority of N_2 from the bed, resulting in CO_2 product purity of over 99%.

The performance of TVSA DAC system relies significantly on the adsorption and heating steps, thus their cut-off criteria were simultaneously compared using contour plots shown in Fig. 5. The simultaneous analysis of these steps revealed that a moderate adsorption criterion of around 65–80% combined with a high heating criterion of 90–95% yielded the highest CO_2 productivity (Fig. 5a). Setting the criteria too high decreased productivity by excessively prolonging the cycle, while setting it too low limited the adsorption uptake and left too much CO_2 loading in the bed after adsorption, also reducing productivity. However, high criteria resulted in the lowest specific energy requirement since they increased the working capacity (Fig. 5b). Although high criteria increased the cycle duration and total energy consumption, the increase in working capacity had a more substantial effect on the specific energy requirement. It should be noted that this model did not account for heat losses, which may increase the specific energy requirement at high heating cut-off criteria.

The selected criteria for sensitivity analyses are summarized in Table 4. To maximize productivity, a base case adsorption cut-off criterion of 75% was initially chosen. However, since this criterion has a significant impact on specific energy requirement and CO_2 productivity, the sensitivity analyses were also performed using 60% and 90% adsorption criteria. It is important to note that the choice of adsorption criterion also affects the optimal values of the process parameters. For the heating step, a 95% cut-off criterion was selected to ensure the best productivity and lowest specific energy requirement. The comparison of adsorption and heating step criteria was conducted using parameter intervals of 5%, indicating that the actual optimum for the heating phase likely falls within the range of 95–100%.

Given the significant impact of the heat transfer coefficient and the reaction rate constants on process performance, a sensitivity analysis on these coefficients was conducted due to the limited available kinetic and heat transfer data for the used adsorbent. Fig. 6 displays the results of this sensitivity analysis. Increasing the heat transfer coefficient from 27.3 W/(m^2K) enhances productivity by facilitating more efficient heat transfer between the gas and the wall, resulting in shorter cycles as the gas reaches the wall temperature more rapidly (Fig. 6a). Conversely, decreasing the heat transfer coefficient significantly reduces productivity, although it has little impact on the specific energy requirement as the working capacity remains constant. The selected heat transfer coefficient corresponds well with the values of 8.6–75 W/(m^2K) reported in other DAC simulation articles [37,38,61].

Experimental correlations allowed to calculate the reaction rate constants for the dry and humid reactions (1) and (2), which were found to be $0.10 \leq k_{f,1} \leq 0.34$ $bar^{-1}s^{-1}(mol/kg)^{1-t1}$ and $1.60 \leq k_{f,2} \leq 12.81$ $bar^{-2}s^{-1}(mol/kg)^{1-t2}$ in the relative humidity range of 0–100%, respectively. In these intervals, the reaction rate constant $k_{f,1}$ has little effect on performance (Fig. 6b), while the reaction rate constant $k_{f,2}$ significantly influences productivity and specific energy requirement (Fig. 6c). Given that these two reaction rate constants define the reaction kinetics of both the dry and humid CO_2 capture reaction mechanisms, altering their relative values changes the extents of the dry and humid CO_2 capture reactions. The humid CO_2 capture reaction is generally more advantageous as it requires fewer amines to capture the same amount of CO_2 based on reaction stoichiometry. Therefore, promoting the humid reaction mechanism increases the adsorption capacity and accelerates the achievement of the designated cut-off points by CO_2 uptake, improving productivity and reducing the specific energy requirement. The reaction rate constant of LDF model $k_{H2O,LDF}$ describing H_2O adsorption was set to constant value of 0.16 1/s, as its fitting contained higher uncertainty and it has minimal impact on performance over the relevant range (Fig. 6d).

4.3. Effect of operating parameters

This section presents the sensitivity analyses demonstrating the effect of operating parameters on DAC system performance, with a primary focus on CO_2 productivity and SER. Additionally, the effects on other important indicators were also considered, including working capacity, cycle time, and absolute energy consumption. The evaluated parameters include CO_2 concentration, relative humidity, temperature, and superficial velocity of the feed air during adsorption, as well as temperature and vacuum pressure during regeneration. By comprehensively examining these variables, the aim is to provide a more detailed understanding of the process performance and its underlying mechanisms.

4.3.1. CO_2 feed concentration

In addition to capturing CO_2 from the atmosphere, which typically has a concentration of around 400 ppm, it is important to examine the performance of DAC systems at other CO_2 feed concentrations. This is particularly relevant for CO_2 capture from enclosed spaces, like buildings, or crowded outdoor places, where the CO_2 concentration can be much higher, potentially yielding cost advantages [65–67]. For instance, a thermodynamic study of the TVSA cycle for DAC revealed that using higher concentrations of CO_2 can significantly reduce the minimum separation work required and improve the second-law efficiency of the process [67].

Fig. 7a illustrates the impact of CO_2 feed concentration on process performance, indicating that increasing the feed concentration can remarkably boost productivity and decrease the SER. For example, when the CO_2 feed concentration is raised from 400 to 800 ppm, productivity increases by 84–86% to 0.51–0.58 $kg_{CO2}/(kg_s d)$, while SER drops by 21–28% to 15.8–22.7 MJ/kg_{CO2}. This enhanced productivity is due to a shorter cycle time, as the adsorption rate rises, and a larger working capacity resulting from higher adsorption equilibrium capacity (Fig. 7b). Both the fastened adsorption rate driven by higher CO_2 concentration and the expanded working capacity seem to play equally vital roles in productivity improvement. The reduction in SER is primarily ascribed to the increase in working capacity but is also influenced by the

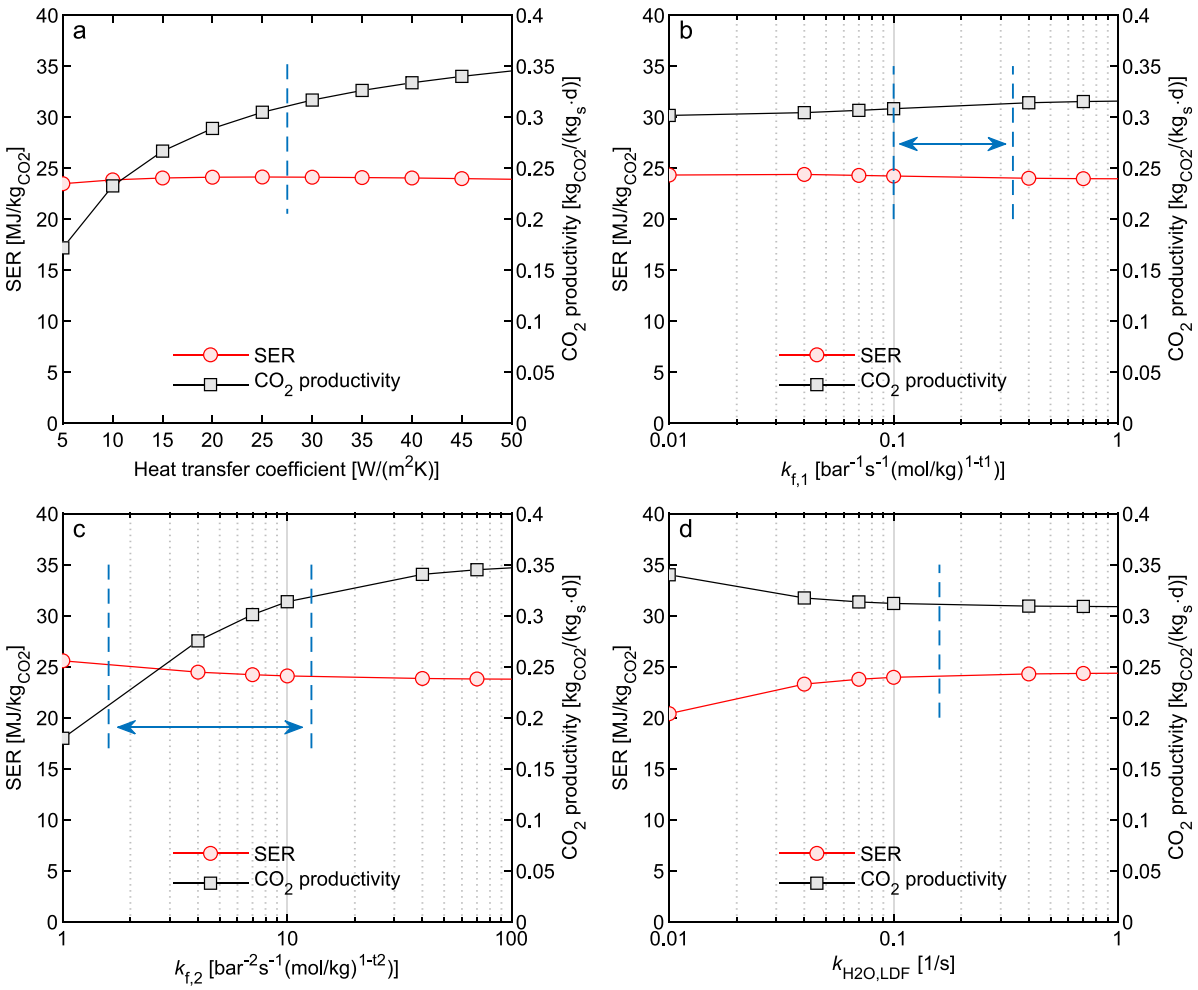

Fig. 6. Effect of (a) heat transfer coefficient, (b) reaction rate constant for reaction (1), (c) reaction rate constant for reaction (2), and (d) LDF kinetic constant of H_2O mass transfer on CO_2 productivity and specific energy requirement. The parameter ranges employed in simulations are indicated by blue dashed lines. The selection of reaction rate constants is explained in Section 3.1. (For interpretation of the references to colour in this figure legend, the reader is referred to the web version of this article.)

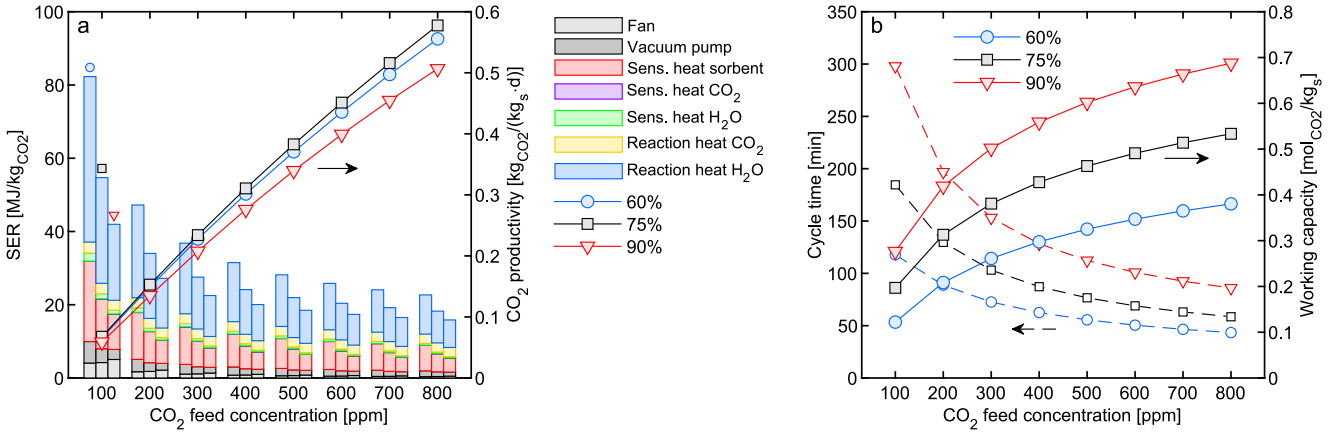

Fig. 7. Effect of CO_2 feed concentration on (a) productivity and specific energy requirement, and (b) working capacity and cycle time. Three adsorption cut-off criteria are compared.

reduced need for mechanical fan and vacuuming energy due to the shortened cycle. However, the impact of reduced energy consumption on SER is found to be small (see Fig. S3 in the SI). Based on these findings, using CO_2 feed concentrations lower than atmospheric CO_2 concentration is not justifiable.

4.3.2. *Relative humidity*

Humidity can either enhance or impede the process of CO_2 adsorption on amine-functionalized adsorbents. Firstly, humidity can significantly increase the CO_2 adsorption capacity due to changes in the reaction mechanism between amines and CO_2 [43,46,68]. Conversely,

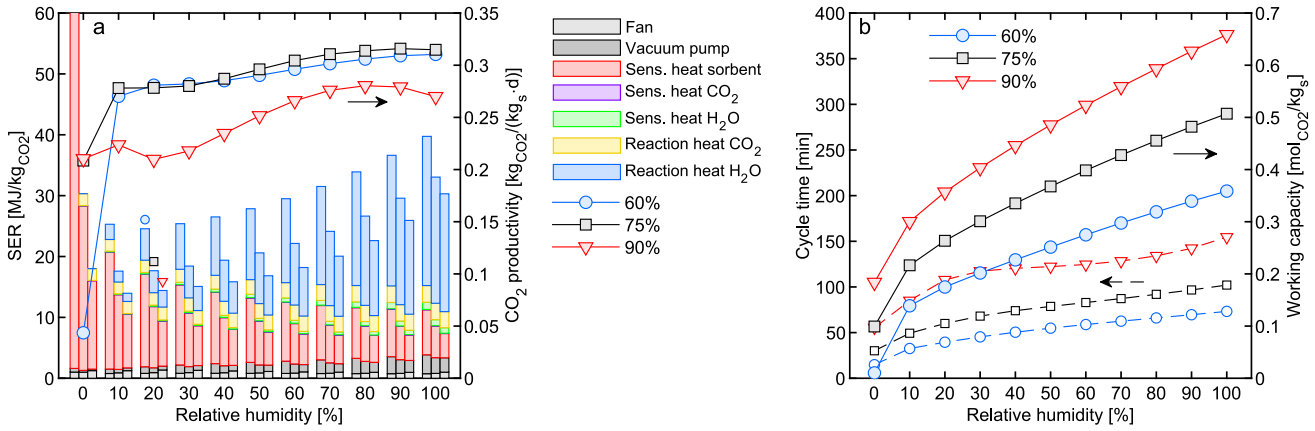

Fig. 8. Effect of humidity on (a) productivity and specific energy requirement, and (b) working capacity and cycle time. Three adsorption cut-off criteria are compared.

humidity can also lead to higher energy penalties induced by H_2O desorption [69], block the CO_2 adsorption sites in the presence of excess moisture [70], cause degradation of some adsorbents [64], or damage process equipment. However, the model did not account for the effect H_2O blocking the adsorption of CO_2, as this is more pronounced in flue gas capture where the H_2O concentration is significantly higher.

Fig. 8a shows the two-way effect of increasing humidity on DAC performance; the CO_2 productivity increases, but so does the specific energy requirement. At 0% relative humidity, the productivity drastically drops from 0.22–0.28 to 0.04–0.21 $kg_{CO2}/(kg_s d)$ compared to 10% relative humidity, particularly when using the 60% adsorption cut-off criterion, due to minimal working capacity. Although higher humidity levels lead to a substantial increase in working capacity, the impact on productivity is minor due to the extended cycle time, which counters the benefits of increased working capacity (Fig. 8b). For instance, working capacity increases from 0.14–0.30 mol_{CO2}/kg_s at 10% RH to 0.34–0.63 mol_{CO2}/kg_s at 90% RH, corresponding to a significant increase of 109–144%, while the productivity only increases by 14–25%. The prolonged cycle time is attributed to the longer duration required to reach the higher adsorption capacity, and the slowing down effect of endothermic H_2O desorption in the heating step. In general, the highest relative humidity levels result in the best productivity, and the utilization of smaller equipment is possible due to reduced requirement for adsorbents. However, it is advisable to maintain relative humidity below 100% to prevent excessive moisture from blocking CO_2 adsorption. Nevertheless, the SER increases by 57–117% from 14.0–25.3 to 30.3–39.7 MJ/kg_{CO2} as the relative humidity increases from 10% to 100%, primarily due to the increasing reaction heat for H_2O desorption and increased mechanical energy demand resulting from a longer cycle (Fig. S4 in the SI). However, at the lowest relative humidity levels, the SER may be outstandingly high despite the total energy consumption being at its lowest because of the reduced working capacity. Therefore, the lowest SER is attainable at relative humidity levels between 10 and 30%.

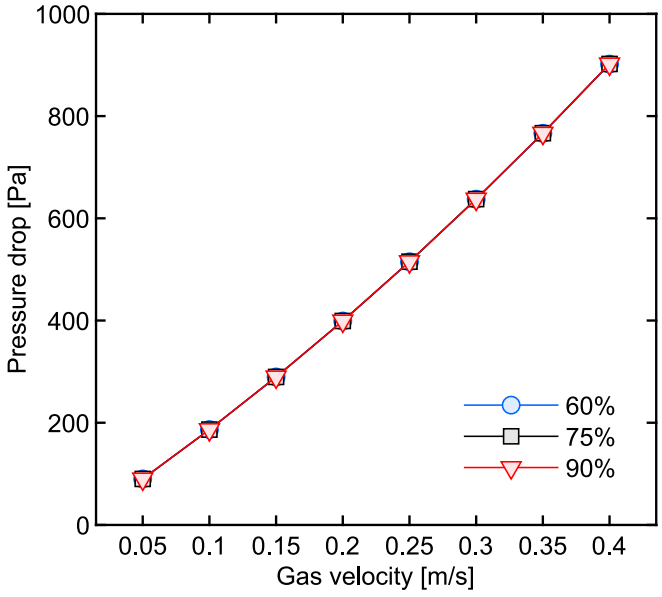

Fig. 10. Effect of superficial gas velocity on pressure drop over the bed.

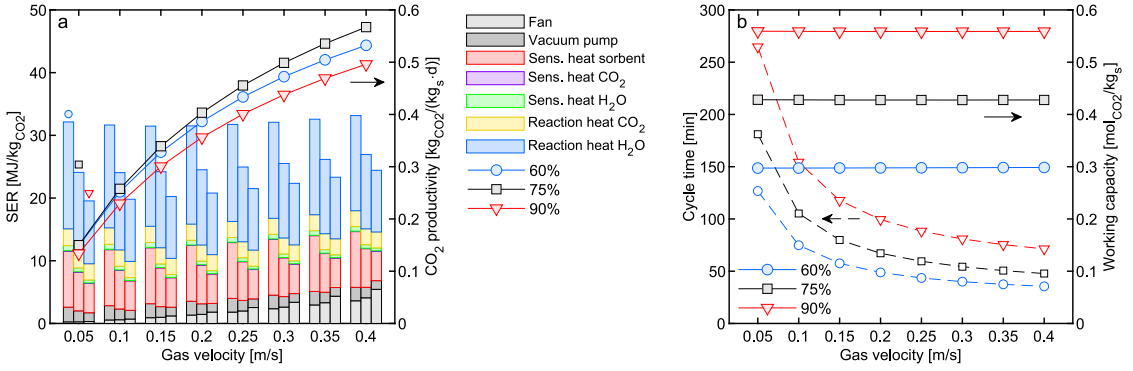

Fig. 9. Effect of superficial gas velocity on (a) productivity and specific energy requirement, and (b) pressure drop and cycle time. Three adsorption cut-off criteria are compared.

4.3.3. Feed gas velocity

Increasing the superficial velocity of the feed gas, which is atmospheric air in DAC, significantly improves CO_2 productivity due to a higher CO_2 supply rate and thus a shorter cycle time (Fig. 9a and 9b). Productivity increases by 278–335% from 0.13–0.15 to 0.50–0.57 $kg_{CO2}/(kg_s d)$ when the feed gas velocity is raised from 0.05 to 0.4 m/s, with the sharpest rise in productivity observed at lower velocities. However, feed gas velocity does not impact working capacity as it does not affect adsorption equilibrium and since the effect of gas velocity on kinetics was not modelled in this work.

It is important to note that the feed gas velocity is limited by pressure drop across the bed, which ranges from 90 to 900 Pa for velocities of 0.05–0.4 m/s (Fig. 10). The superficial gas velocities typically range between 0.05 and 1 m/s in the literature related to fixed bed DAC designs and modelling [36,38,71], while other types of contactors such as monolithic bed can enable even higher velocities due to smaller flow resistance [72]. Economically feasible DAC systems generally require low pressure drops as large volumes of air need to pass through the systems due to the low atmospheric CO_2 concentration. Ideally, the pressure drop across the bed should be less than 300 Pa [41,50]. Too high pressure drop can limit the applicability of industrial air blowers, presenting an upper limit to air flow and thickness of the adsorbent bed, and may thus become a crucial bottleneck in the productivity of the DAC system. Additionally, the pressure drop of the system is underestimated by the model, which only accounts for the pressure drop across the adsorbent bed while losses and friction caused by other system components and piping are neglected.

The increasing pressure drop results in higher energy consumption by the air fan (Fig. S5 in the SI), leading to a 122–299% increase in mechanical energy related SER from 1.7–2.6 to 5.8–6.8 MJ/kg_{CO2} within the studied parameter range. In the same range, the total SER remains relatively stable, increasing only by 3–25% from 19.5–32.2 to 24.4–33.2 MJ/kg_{CO2}, as the compensating effect of shorter adsorption time slows down the increase of SER. However, the increased mechanical energy demand may cause high additional costs for DAC systems that use inexpensive heat sources (e.g. waste heat) to cover their heat demand. Based on these findings, it is beneficial to use a higher gas supply velocity for increased productivity as long as the resulting pressure drop does not exceed the system limitations and increase the total operating cost too much due to the increase in mechanical energy consumption.

4.3.4. Adsorption temperature

The effect of adsorption temperature on CO_2 productivity exhibits a distinct behaviour compared to other operating parameters. Fig. 11a shows that clear maxima in CO_2 productivity are observed at adsorption temperatures that are highly dependent on the adsorption cut-off criterion. Although the highest working capacities are achieved at the lowest adsorption temperatures (Fig. 11b), the peaks in productivity are observed at 10 °C, 20 °C, and 25 °C for 60%, 75%, and 90% cut-off criteria, respectively. Notably, the highest productivity of 0.35 $kg_{CO2}/(kg_s d)$ is obtained at 10 °C with a 60% cut-off criterion, which contrasts with the trend observed for other operating parameters where the 60% cut-off criterion resulted in intermediate productivity levels. However, the occurrence of clearly observed productivity maxima, rather than ever-increasing productivity with decreasing adsorption temperature, is somewhat artificial since lower adsorption temperatures lead to longer adsorption and cycle times, which ultimately result in lower productivity when using a strictly constant adsorption cut-off criterion. Thus, the best productivity within the studied adsorption temperature range would be achieved at the lowest temperature of 0 °C using a sufficiently low adsorption cut-off criterion below 60%, which compensates for longer cycle time. Conversely, overly high adsorption temperatures decrease productivity due to lower working capacity.

Lower adsorption temperatures also result in lower SER, as long as cycle time does not excessively increase, leading to higher fan electricity consumption. While the lowest cut-off criterion of 60% is beneficial for productivity up to 20 °C, it results in higher SER compared to higher cut-off criteria at adsorption temperatures higher than 5 °C. The main reason for this is that the lowest cut-off criterion also yields the lowest working capacities. Especially at higher adsorption temperatures above 30 °C, the SER increases significantly due to severely reduced working capacity. Thus, to optimize both productivity and SER, it is advantageous to maintain adsorption temperatures at 25 °C or lower.

It is important to note that the adsorption temperature is highly dependent on the weather conditions at the location of the DAC system. Varying the temperature of the feed air is impractical and uneconomical due to the large volumetric supply air flow. While cooling the adsorption bed below atmospheric conditions may be beneficial in terms of productivity and SER based on the results above, this causes an additional energy cost and may require additional investment in cooler units. Placing the system in a geographically cooler area may increase productivity and decrease SER, but other factors such as affordable heat availability should also be considered. Additionally, temperatures below 0 °C can cause freezing problems due to humidity in the air.

4.3.5. Desorption temperature

Fig. 12a shows that both productivity and SER improve as desorption temperature increases. The primary reason for this is that higher desorption temperature leads to higher working capacity, as shown in Fig. 12b. For example, increasing desorption temperature from 60 to 100 °C increases the CO_2 productivity from 0.01–0.07 to 0.28–0.31 $kg_{CO2}/(kg_s d)$, while working capacity increases from 0.003–0.11 to 0.30–0.56 mol_{CO2}/kg_s. However, the productivity increase is slightly

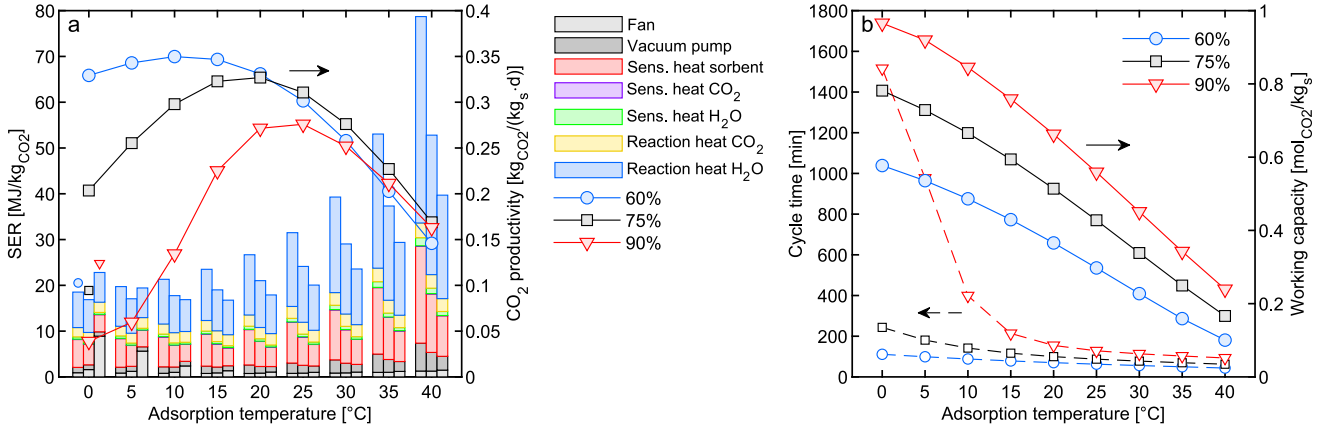

Fig. 11. Effect of adsorption temperature on (a) productivity and specific energy requirement, and (b) working capacity and cycle time. Three adsorption cut-off criteria are compared.

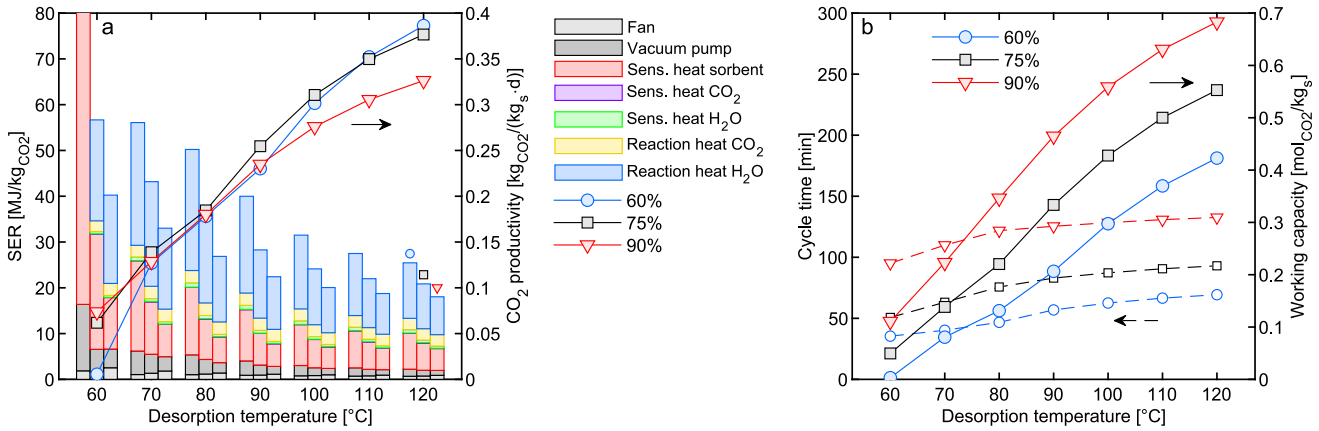

Fig. 12. Effect of desorption temperature on (a) productivity and specific energy requirement, and (b) working capacity and total energy requirement. Three adsorption cut-off criteria are compared.

diminished by an extended total cycle time, since while the heating step speeds up at higher desorption temperatures, the more complete regeneration of the adsorbent bed leads to a longer subsequent adsorption step. The optimal adsorption cut-off criterion for maximizing productivity depends on the desorption temperature. For instance, the highest working capacity and thus the best productivity at 60 °C is reached with 90% criterion, while the 60% criterion is preferable at desorption temperatures above 110 °C, where short cycle time outweighs high working capacity.

Increasing working capacity can also significantly reduce SER, although total energy consumption increases with increasing desorption temperature due to higher reaction and sensible heats (see Fig. S7 in the SI). The total SER is almost halved with a desorption temperature increase from 60 to 100 °C. However, the SER decreases only slightly at higher desorption temperatures than 100 °C, settling to 18.0–25.5 MJ/kg$_{CO2}$ at 120 °C. With even higher desorption temperatures, the SER is expected to increase due to diminished returns in working capacity.

Despite the advantages of elevated desorption temperature, the temperature is limited by the available heat sources and the stability and material properties of the amine-based adsorbents. Adsorbent degradation may easily cause adsorbent replacements to become the most significant cost component in DAC and may cause environmental drawbacks in the scale-up of DAC. Thus, it is important to carefully weigh the benefits of a higher temperature against the temperature restrictions. For instance, utilizing inexpensive waste heat can significantly reduce total costs or even be a prerequisite for the cost competitiveness of the DAC system. In terms of optimal productivity and SER, the highest studied desorption temperature of 120 °C is the best option with all cut-off criteria. However, some adsorbents may suffer significant oxidative or other forms of degradation already at temperatures nearing 100 °C [64,73]. On the other hand, based on the results of this study, using too low desorption temperature at 60–70 °C severely limits the productivity of DAC, and may result in very high SER.

4.3.6. *Vacuum pressure*

Fig. 13a indicates that the highest productivity of 0.34 kg$_{CO2}$/(kg$_s$d) is attained at the lowest examined vacuum pressure of 0.05 bar. This is because a lower vacuum pressure results in a lower equilibrium desorption uptake according to the isotherm, and thus a higher working capacity, as demonstrated in Fig. 13b.

However, decreasing the vacuum pressure level increases the electricity consumption of the vacuum pump (Fig. S8 in the SI), which contributes to the growing share of vacuum energy consumption in the SER. Notably, the SER reaches its peak of 21.9–37.1 MJ/kg$_{CO2}$ with all cut-off criteria at a vacuum pressure of 0.25 bar and declines on either side of this point, albeit only slightly at higher vacuum pressures. At lower vacuum pressures, the decrease is due to the increased working capacity, while at higher pressures, the cycle duration is slightly shortened, leading to decreased energy requirement. The regeneration phase ends with a higher CO_2 uptake at higher vacuum pressure levels, leading to a shorter adsorption phase as adsorption cut-off criterion is reached more quickly. The lowest SER of 19.7 MJ/kg$_{CO2}$ is obtained with 90% cut-off criterion at 0.05 bar pressure.

Based on these results, the best performance of DAC system is achieved with the lowest possible vacuum pressure, subject to the minimum achievable pressure of the vacuum pump. However, it is worth noting

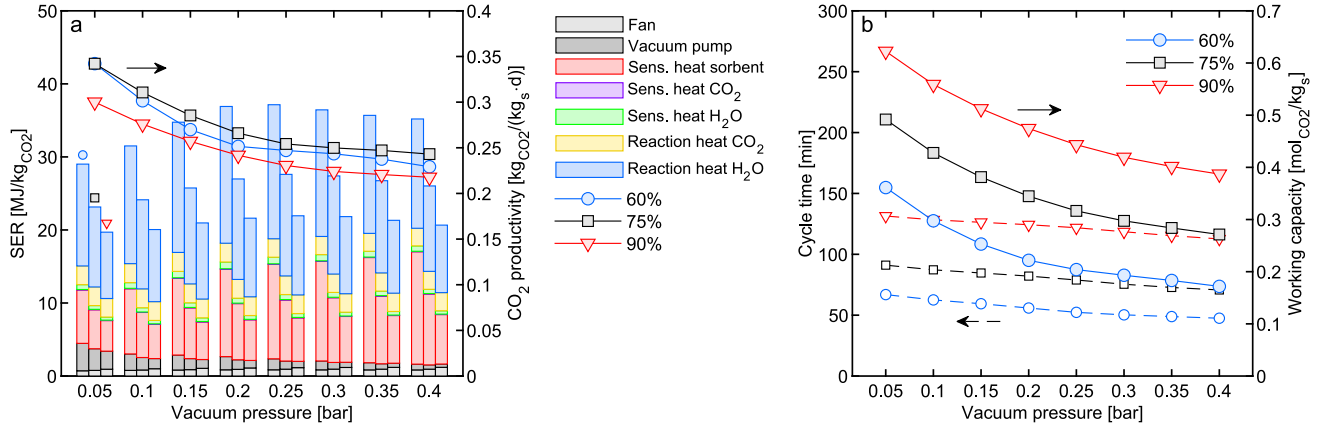

Fig. 13. Effect of vacuum pressure on (a) productivity and specific energy requirement, and (b) working capacity and cycle time. Three adsorption cut-off criteria are compared.

that the vacuum pump's efficiency may decrease more than anticipated at extremely low pressures.

5. Conclusions

In this study, the performance of an adsorbent-based DAC process was investigated using a dynamic fixed-bed model of a TVSA process. A previously reported kinetic model was utilized for CO_2 adsorption that takes into account the impact of humidity on CO_2 adsorption on amine-functionalized adsorbents. The dynamic model was validated with experimental data, and the influence of the used heat transfer and kinetic parameters were examined. The effects of various cycle step cut-off criteria and operating parameters on DAC performance were investigated and presented as primary results.

Optimizing the durations of the adsorption and regeneration phases was found to be crucial for improving DAC process performance. The lowest SER was generally achieved by driving both phases towards an almost equilibrium state using cut-off criteria of 90–100%. On the other hand, the best CO_2 productivity was obtained by cutting the adsorption phase at 60–75% to prevent the cycle from becoming inefficient due to excessive duration. This implies that a trade-off between productivity and SER must be made.

Making appropriate choices of operating parameters were also found to significantly improve the performance of the DAC process. Using a CO_2 source with a concentration of a few hundred ppm above the atmospheric CO_2 level greatly enhanced productivity and reduced SER by accelerating the adsorption phase and increasing the working capacity of the cycle. Similarly, increasing the air velocity also improved productivity by accelerating CO_2 adsorption, but at the cost of higher energy consumption by the air blower because of steeply rising pressure drop. Additionally, a high relative humidity of the feed increased the working capacity of the cycle, but only marginally improved productivity due to the opposing effect of increased cycle duration. However, humidity incurred a higher energy penalty due to the heat requirement of H_2O desorption. Operating the DAC system at a low adsorption temperature and high desorption temperature resulted in the highest working capacity of the cycle, improving both productivity and SER. Nevertheless, there are limitations to the operating temperatures. Lowering the adsorption temperature below 0 °C may cause issues due to moisture freezing, while raising the desorption temperature above 100 °C typically causes stability problems for many amine-based adsorbents and limits the applicable heat source. Lastly, lowering the vacuum pressure improved productivity and potentially reduced SER due to increased working capacity, despite the increase in electricity consumption by the vacuum pump.

The findings of this study emphasize the significant impact of three factors on the performance and cost-effectiveness of the DAC system, namely the placement of the DAC unit, weather conditions, and process parameter selection. Placing the DAC unit in a geographically cooler climate could be advantageous, because cooling large volumes of feed air is not economically feasible. In addition, integrating the DAC process with inexpensive heat sources that are available at approximately 100 °C would considerably reduce total energy costs, as thermal energy accounted for 57–99% of the SER in the analyses. By optimizing the feed gas velocity and vacuum pressure, the consumption of electrical energy could be minimized. Finally, the utilization of sources with higher CO_2 concentrations, such as inhabited environments, was found to be profitable. These individual methods could increase the CO_2 productivity of the DAC process up to 0.58 $kg_{CO2}/(kg_s d)$ and reduce the SER to 14.0 MJ/kg_{CO2}.

It is important to note that the conducted analyses only focused on the effects of individual operating and model parameters, and thus cannot be used alone for comprehensive optimization of the DAC system. A more multidimensional approach would be required, including examination of trade-offs between productivity, SER, and various constraints, as well as consideration of total costs in addition to the aforementioned performance indicators. Such multidimensional optimization would enable even better overall performance. Nevertheless, this study provides valuable insights into DAC process optimization and strengthens the foundation for further research and development in this area.

CRediT authorship contribution statement

Aaro Luukkonen: Conceptualization, Methodology, Software, Investigation, Writing – original draft, Visualization. **Jere Elfving:** Conceptualization, Methodology, Software, Resources, Writing – review & editing, Supervision, Project administration, Funding acquisition. **Eero Inkeri:** Software, Writing – review & editing.

Declaration of Competing Interest

The authors declare that they have no known competing financial interests or personal relationships that could have appeared to influence the work reported in this paper.

Data availability

Data will be made available on request.

Acknowledgements

This study was conducted as a part of the DAC2.0 project funded by the Academy of Finland under grant number 329312.

Appendix A. Supplementary data

Supplementary data to this article can be found online at https://doi.org/10.1016/j.cej.2023.144525.

References

[1] M. Pathak, R. Slade, R. Pichs-Madruga, D. Ürge-Vorsatz, P.R. Shukla, J. Skea, T. Summary, Technical summary, in: Climate Change 2022: Mitigation of Climate Change. Contribution of Working Group III to the Sixth Assessment Report of the Intergovernmental Panel on Climate Change, 2022, https://doi.org/10.1017/9781009157926.002.

[2] UNEP, Emissions Gap Report 2022: The Closing Window — Climate crisis calls for rapid transformation of societies, Nairobi, 2022. https://www.unep.org/resources/emissions-gap-report-2022 (accessed April 4, 2023).

[3] C. Breyer, M. Fasihi, C. Bajamundi, F. Creutzig, Direct air capture of CO_2: A key technology for ambitious climate change mitigation, Joule 3 (2019) 2053–2057, https://doi.org/10.1016/J.JOULE.2019.08.010.

[4] IEA, Direct Air Capture: A key technology for net zero, Paris, 2022. https://www.iea.org/reports/direct-air-capture-2022 (accessed August 12, 2022).

[5] C. Beuttler, L. Charles, J. Wurzbacher, The role of direct air capture in mitigation of anthropogenic greenhouse gas emissions, Front. Clim. 1 (2019) 10, https://doi.org/10.3389/FCLIM.2019.00010.

[6] IEA, Net Zero by 2050. A Roadmap for the Global Energy Sector, Paris, 2021. https://www.iea.org/reports/net-zero-by-2050 (accessed August 19, 2022).

[7] M. Bui, C.S. Adjiman, A. Bardow, E.J. Anthony, A. Boston, S. Brown, P.S. Fennell, S. Fuss, A. Galindo, L.A. Hackett, J.P. Hallett, H.J. Herzog, G. Jackson, J. Kemper, S. Krevor, G.C. Maitland, M. Matuszewski, I.S. Metcalfe, C. Petit, G. Puxty, J. Reimer, D.M. Reiner, E.S. Rubin, S.A. Scott, N. Shah, B. Smit, J.P.M. Trusler, P. Webley, J. Wilcox, N. Mac Dowell, Carbon capture and storage (CCS): the way forward, Energy Environ Sci. 11 (2018) 1062–1176, https://doi.org/10.1039/C7EE02342A.

[8] G. Realmonte, L. Drouet, A. Gambhir, J. Glynn, A. Hawkes, A.C. Köberle, M. Tavoni, An inter-model assessment of the role of direct air capture in deep mitigation pathways, Nat. Commun. 2019 10:1. 10 (2019) 1–12. https://doi.org/10.1038/s41467-019-10842-5.

[9] S.M. Smith, O. Geden, M. Gidden, W.F. Lamb, J.C. Minx, I. Iv, G.F. Nemet, C. Powis, R. Bellamy, M. Callaghan, A. Cowie, E. Cox, S. Fuss, T. Gasser, G. Grassi, J. Greene, S. Lück, A. Mohan, F. Müller-Hansen, G. Peters, Y. Pratama, T. Repke, K. Riahi, F. Schenuit, J. Steinhauser, J. Strefler, J.M. Valenzuela, accessed January 23, 2023, The State of Carbon Dioxide Removal (2023), https://www.stateofcdr.org.

[10] IEAGHG, Assessing the Techno-Economic Performance, Opportunities and Challenges of Mature and Nearly-mature Negative Emissions Technologies (NETs), 2021. https://ieaghg.org/publications/technical-reports/reports-list/9-technical

-reports/1056-2021-04-techno-economic-performance-opportunities-and-challenges-of-nets (accessed February 2, 2023).
[11] National Academies of Sciences, Negative Emissions Technologies and Reliable Sequestration: A Research Agenda, National Academies Press, Washington, 2019 https://doi.org/10.17226/25259.
[12] EASAC, Negative emission technologies: What role in meeting Paris Agreement targets?, German National Academy of Sciences Leopoldina, Halle, 2018. https://easac.eu/fileadmin/PDF_s/reports_statements/Negative_Carbon/EASAC_Report_on_Negative_Emission_Technologies.pdf (accessed August 19, 2022).
[13] S. Fuss, W.F. Lamb, M.W. Callaghan, J. Hilaire, F. Creutzig, T. Amann, T. Beringer, W. De Oliveira Garcia, J. Hartmann, T. Khanna, G. Luderer, G.F. Nemet, J. Rogelj, P. Smith, J.V. Vicente, J. Wilcox, M. Del Mar Zamora, J.C.M. Dominguez, Negative emissions - Part 2: Costs, potentials and side effects, Environ. Res. Lett. 13 (2018), 063002, https://doi.org/10.1088/1748-9326/aabf9f.
[14] F. Kazemifar, A review of technologies for carbon capture, sequestration, and utilization: Cost, capacity, and technology readiness, Greenhouse Gases: Sci. Technol. 12 (2022) 200–230, https://doi.org/10.1002/GHG.2131.
[15] IEA, CCUS in Clean Energy Transitions, Paris, 2020. https://www.iea.org/reports/ccus-in-clean-energy-transitions (accessed August 19, 2022).
[16] L. Fu, Z. Ren, W. Si, Q. Ma, W. Huang, K. Liao, Z. Huang, Y. Wang, J. Li, P. Xu, Research progress on CO_2 capture and utilization technology, J. CO_2 Util. 66 (2022), 102260, https://doi.org/10.1016/J.JCOU.2022.102260.
[17] L. Jiang, W. Liu, R.Q. Wang, A. Gonzalez-Diaz, M.F. Rojas-Michaga, S. Michailos, M. Pourkashanian, X.J. Zhang, C. Font-Palma, Sorption direct air capture with CO_2 utilization, Prog Energy Combust Sci. 95 (2023), 101069, https://doi.org/10.1016/J.PECS.2022.101069.
[18] E.S. Sanz-Pérez, C.R. Murdock, S.A. Didas, C.W. Jones, Direct capture of CO_2 from ambient air, Chem Rev. 116 (2016) 11840–11876, https://doi.org/10.1021/acs.chemrev.6b00173.
[19] X. Shi, H. Xiao, H. Azarabadi, J. Song, X. Wu, X. Chen, K.S. Lackner, Sorbents for the direct capture of CO_2 from ambient air, Angew. Chem. 132 (2020) 7048–7072, https://doi.org/10.1002/ange.201906756.
[20] D.W. Keith, G. Holmes, D. St, K.H. Angelo, A process for capturing CO_2 from the atmosphere, Joule 2 (2018) 1573–1594, https://doi.org/10.1016/j.joule.2018.05.006.
[21] K. Lackner H.-J. Ziock P. Grimes Carbon Dioxide Extraction From Air: Is It An Option? in: 24th Annual Technical Conference on Coal Utilization and Fuel Systems 1999 Los Alamos.
[22] R. Socolow, M. Desmond, R. Aines, J. Blackstock, O. Bolland, T. Kaarsberg, N. Lewis, Direct air capture of CO_2 with chemicals: A technology assessment for the APS Panel on Public Affairs, 2011.
[23] R. Custelcean, K.A. Garrabrant, P. Agullo, N.J. Williams, Direct air capture of CO_2 with aqueous peptides and crystalline guanidines, Cell Rep Phys Sci. 2 (2021), 100385, https://doi.org/10.1016/J.XCRP.2021.100385.
[24] X. Zhu, W. Xie, J. Wu, Y. Miao, C. Xiang, C. Chen, B. Ge, Z. Gan, F. Yang, M. Zhang, D. O'Hare, J. Li, T. Ge, R. Wang, Recent advances in direct air capture by adsorption, Chem. Soc. Rev. 51 (2022) 6574–6651, https://doi.org/10.1039/D1CS00970B.
[25] T. Gelles, S. Lawson, A.A. Rownaghi, F. Rezaei, Recent advances in development of amine functionalized adsorbents for CO_2 capture, Adsorption 26 (2020) 5–50, https://doi.org/10.1007/s10450-019-00151-0.
[26] M. Yang, C. Ma, M. Xu, S. Wang, L. Xu, Recent advances in CO_2 adsorption from air: a review, Curr. Pollut. Rep. 5 (2019) 272–293, https://doi.org/10.1007/s40726-019-00128-1.
[27] S.A. Didas, S. Choi, W. Chaikittisilp, C.W. Jones, Amine-oxide hybrid materials for CO_2 capture from ambient air, Acc. Chem. Res. 48 (2015) 2680–2687, https://doi.org/10.1021/ACS.ACCOUNTS.5B00284.
[28] J. Elfving, J. Kauppinen, M. Jegoroff, V. Ruuskanen, L. Järvinen, T. Sainio, Experimental comparison of regeneration methods for CO_2 concentration from air using amine-based adsorbent, Chem. Eng. J. 404 (2021), 126337, https://doi.org/10.1016/j.cej.2020.126337.
[29] R.P. Wijesiri, G.P. Knowles, H. Yeasmin, A.F.A. Hoadley, A.L. Chaffee, Desorption process for capturing CO_2 from air with supported amine sorbent, Ind. Eng. Chem. Res. 58 (2019) 15606–15618, https://doi.org/10.1021/acs.iecr.9b03140.
[30] M.J. Bos, V. Kroeze, S. Sutanto, D.W.F. Brilman, Evaluating regeneration options of solid amine sorbent for CO_2 removal, Ind Eng Chem Res. 57 (2018) 11141–11153, https://doi.org/10.1021/acs.iecr.8b00768.
[31] IEAGHG, Global Assessment of Direct Air Capture Costs, 2021. www.ieaghg.org.
[32] M. Fasihi, O. Efimova, C. Breyer, Techno-economic assessment of CO_2 direct air capture plants, J. Clean. Prod. 224 (2019) 957–980, https://doi.org/10.1016/j.jclepro.2019.03.086.
[33] R. Chauvy, L. Dubois, Life cycle and techno-economic assessments of direct air capture processes: An integrated review, Int. J. Energy Res. 46 (2022) 10320–10344, https://doi.org/10.1002/ER.7884.
[34] K.S. Lackner, H. Azarabadi, Buying down the cost of direct air capture, Ind. Eng. Chem. Res. 60 (2021) 8196–8208, https://doi.org/10.1021/ACS.IECR.0C04839.
[35] H. Azarabadi, K.S. Lackner, A sorbent-focused techno-economic analysis of direct air capture, Appl. Energy 250 (2019) 959–975, https://doi.org/10.1016/J.APENERGY.2019.04.012.
[36] H.M. Schellevis, T.N. van Schagen, D.W.F. Brilman, Process optimization of a fixed bed reactor system for direct air capture, Int. J. Greenhouse Gas Control 110 (2021), 103431, https://doi.org/10.1016/J.IJGGC.2021.103431.
[37] V. Stampi-Bombelli, M. van der Spek, M. Mazzotti, Analysis of direct capture of CO_2 from ambient air via steam-assisted temperature–vacuum swing adsorption, Adsorption. 26 (2020) 1183–1197. https://doi.org/-10.1007/s10450-020-00249-w.
[38] X. Zhu, T. Ge, F. Yang, R. Wang, Design of steam-assisted temperature vacuum-swing adsorption processes for efficient CO_2 capture from ambient air, Renew. Sustain. Energy Rev. 137 (2021), 110651, https://doi.org/10.1016/j.rser.2020.110651.
[39] F. Sabatino, A. Grimm, F. Gallucci, M. van Sint Annaland, G.J. Kramer, M. Gazzani, A comparative energy and costs assessment and optimization for direct air capture technologies, Joule. 5 (2021) 2047–2076. https://doi.org/10.1016/j.joule.2021.05.023.
[40] J.A. Wurzbacher, C. Gebald, S. Brunner, A. Steinfeld, Heat and mass transfer of temperature–vacuum swing desorption for CO_2 capture from air, Chem. Eng. J. 283 (2016) 1329–1338, https://doi.org/10.1016/j.cej.2015.08.035.
[41] A. Sinha, M.J. Realff, A parametric study of the techno-economics of direct CO_2 air capture systems using solid adsorbents, AIChE J. 65 (2019) e16607.
[42] J. Young, E. García-Díez, S. Garcia, M. Van Der Spek, The impact of binary water–CO2 isotherm models on the optimal performance of sorbent-based direct air capture processes, Energy Environ Sci. 14 (2021) 5377–5394, https://doi.org/10.1039/D1EE01272J.
[43] J.M. Kolle, M. Fayaz, A. Sayari, Understanding the effect of water on CO_2 adsorption, Chem. Rev. 121 (2021) 7280–7345, https://doi.org/10.1021/acs.chemrev.0c00762.
[44] M.J. Bos, S. Pietersen, D.W.F. Brilman, Production of high purity CO_2 from air using solid amine sorbents, Chem. Eng. Sci.: X 2 (2019), 100020, https://doi.org/10.1016/J.CESX.2019.100020.
[45] N.K. Sandhu, D. Pudasainee, P. Sarkar, R. Gupta, Steam regeneration of polyethylenimine-impregnated silica sorbent for postcombustion CO_2 capture: A multicyclic study, Ind. Eng. Chem. Res. 55 (2016) 2210–2220, https://doi.org/10.1021/acs.iecr.5b04741.
[46] J. Elfving, T. Sainio, Kinetic approach to modelling CO_2 adsorption from humid air using amine-functionalized resin: Equilibrium isotherms and column dynamics, Chem. Eng. Sci. 246 (2021), 116885, https://doi.org/10.1016/j.ces.2021.116885.
[47] J. Elfving, C. Bajamundi, J. Kauppinen, Characterization and performance of direct air capture sorbent, Energy Procedia 114 (2017) 6087–6101, https://doi.org/10.1016/j.egypro.2017.03.1746.
[48] J. Elfving, Direct capture of CO_2 From Air Using Amine-Functionalized Resin - Effect of Humidity in Modelling and Evaluation of Process Concepts, Ph.D. Dissertation, Lappeenranta-Lahti University of Technology LUT, 2021. https://lutpub.lut.fi/handle/10024/163524 (accessed March 29, 2022).
[49] C.J.E. Bajamundi, J. Koponen, V. Ruuskanen, J. Elfving, A. Kosonen, J. Kauppinen, J. Ahola, Capturing CO_2 from air: Technical performance and process control improvement, J. CO_2 Util. 30 (2019) 232–239, https://doi.org/10.1016/J.JCOU.2019.02.002.
[50] C. Gebald, N. Piatkowski, T. Rüesch, J.A. Wurzbacher, Low-pressure drop structure of particle adsorbent bed for adsorption gas separation process, WO2014170184A1, 2014.
[51] J.A. Wurzbacher, N. Repond, T. Ruesch, S. Sauerbeck, C. Gebald, Low-pressure drop structure of particle adsorbent bed for improved adsorption gas separation process, WO/2018/083109, 2017.
[52] K. Li, J.D. Kress, D.S. Mebane, The mechanism of CO_2 adsorption under dry and humid conditions in mesoporous silica-supported amine sorbents, J. Phys. Chem. C 120 (2016) 23683–23691, https://doi.org/10.1021/acs.jpcc.6b08808.
[53] E.F. da Silva, H.F. Svendsen, Computational chemistry study of reactions, equilibrium and kinetics of chemical CO_2 absorption, Int. J. Greenhouse Gas Control 1 (2007) 151–157, https://doi.org/10.1016/S1750-5836(07)00022-9.
[54] M. Sardo, R. Afonso, J. Juźków, M. Pacheco, M. Bordonhos, M.L. Pinto, J.R. B. Gomes, L. Mafra, Unravelling moisture-induced CO_2 chemisorption mechanisms in amine-modified sorbents at the molecular scale, J. Mater. Chem. A Mater. 9 (2021) 5542–5555, https://doi.org/10.1039/D0TA09808F.
[55] S. Sircar, J.R. Hufton, Why does the linear driving force model for adsorption kinetics work? Adsorption 6 (2000) 137–147, https://doi.org/10.1023/A:1008965317983.
[56] E.J. Quirijns, A.J.B. Van Boxtel, W.K.P. Van Loon, G. Van Straten, Sorption isotherms, GAB parameters and isosteric heat of sorption, J. Sci. Food Agric. 85 (2005) 1805–1814, https://doi.org/10.1002/jsfa.2140.
[57] P. Bollini, N.A. Brunelli, S.A. Didas, C.W. Jones, Dynamics of CO_2 adsorption on amine adsorbents. 1. Impact of heat effects, Ind. Eng. Chem. Res. 51 (2012) 15145–15152, https://doi.org/10.1021/ie301790a.
[58] M.S. Shafeeyan, W.M.A. Wan Daud, A. Shamiri, A review of mathematical modeling of fixed-bed columns for carbon dioxide adsorption, Chem. Eng. Res. Design 92 (2014) 961–988, https://doi.org/10.1016/j.cherd.2013.08.018.
[59] D.M. Ruthven, Principles of Adsorption and Adsorption Processes, John Wiley & Sons, 1984 https://doi.org/0-471-86606-7.
[60] S.O. Rastegar, T. Gu, Empirical correlations for axial dispersion coefficient and Peclet number in fixed-bed columns, J Chromatogr A. 1490 (2017) 133–137, https://doi.org/10.1016/j.chroma.2017.02.026.
[61] R. Haghpanah, A. Majumder, R. Nilam, A. Rajendran, S. Farooq, I.A. Karimi, M. Amanullah, Multiobjective optimization of a four-step adsorption process for postcombustion CO_2 capture via finite volume simulation, Ind. Eng. Chem. Res. 52 (2013) 4249–4265, https://doi.org/10.1021/ie302658y.
[62] E. Sonnleitner, G. Schöny, H. Hofbauer, Assessment of zeolite 13X and Lewatit® VP OC 1065 for application in a continuous temperature swing adsorption process for biogas upgrading, Biomass Convers. Biorefin. 8 (2018) 379–395, https://doi.org/10.1007/S13399-017-0293-3.
[63] S. Krishnamurthy, V.R. Rao, S. Guntuka, P. Sharratt, R. Haghpanah, A. Rajendran, M. Amanullah, I.A. Karimi, S. Farooq, CO_2 capture from dry flue gas by vacuum swing adsorption: A pilot plant study, AIChE J. 60 (2014) 1830–1842, https://doi.org/10.1002/AIC.14435.

[64] M. Jahandar Lashaki, S. Khiavi, A. Sayari, Stability of amine-functionalized CO_2 adsorbents: a multifaceted puzzle, Chem. Soc. Rev. 48 (2019) 3320–3405, https://doi.org/10.1039/C8CS00877A.
[65] M.K. Kim, L. Baldini, H. Leibundgut, J.A. Wurzbacher, N. Piatkowski, A novel ventilation strategy with CO_2 capture device and energy saving in buildings, Energy Build. 87 (2015) 134–141, https://doi.org/10.1016/J.ENBUILD.2014.11.017.
[66] T.S. Lee, J.H. Cho, S.H. Chi, Carbon dioxide removal using carbon monolith as electric swing adsorption to improve indoor air quality, Build Environ. 92 (2015) 209–221, https://doi.org/10.1016/J.BUILDENV.2015.04.028.
[67] R. Zhao, L. Liu, L. Zhao, S. Deng, S. Li, Y. Zhang, H. Li, Thermodynamic exploration of temperature vacuum swing adsorption for direct air capture of carbon dioxide in buildings, Energy Convers. Manag. 183 (2019) 418–426, https://doi.org/10.1016/J.ENCONMAN.2019.01.009.
[68] J.A. Wurzbacher, C. Gebald, N. Piatkowski, A. Steinfeld, Concurrent separation of CO_2 and H_2O from air by a temperature-vacuum swing adsorption/desorption cycle, Environ. Sci. Technol. 46 (2012) 9191–9198, https://doi.org/10.1021/ES301953K.
[69] C. Drechsler, D.W. Agar, Investigation of water co-adsorption on the energy balance of solid sorbent based direct air capture processes, Energy 192 (2020), 116587, https://doi.org/10.1016/J.ENERGY.2019.116587.
[70] H. Zhang, A. Goeppert, G.A. Olah, G.K.S. Prakash, Remarkable effect of moisture on the CO2 adsorption of nano-silica supported linear and branched polyethylenimine, J. CO2 Util. 19 (2017) 91–99, https://doi.org/10.1016/J.JCOU.2017.03.008.
[71] Q. Yu, W. Brilman, A radial flow contactor for ambient air CO_2 capture, Appl. Sci. 10 (2020) 1080, https://doi.org/10.3390/app10031080.
[72] A. Sinha, L.A. Darunte, C.W. Jones, M.J. Realff, Y. Kawajiri, Systems design and economic analysis of direct air capture of CO_2 through temperature vacuum swing adsorption using MIL-101(Cr)-PEI-800 and mmen-Mg_2(dobpdc) MOF adsorbents, Ind. Eng. Chem. Res. 56 (2017) 750–764, https://doi.org/10.1021/acs.iecr.6b03887.
[73] Q. Yu, J.D.L.P. Delgado, R. Veneman, D.W.F. Brilman, Stability of a benzyl amine based CO_2 capture adsorbent in view of regeneration strategies, Ind. Eng. Chem. Res. 56 (2017) 3259–3269, https://doi.org/10.1021/ACS.IECR.6B04645.